Effects of long-lived 10 MeV-scale sterile neutrinos on primordial elemental abundances and the effective neutrino number

Hiroyuki Ishida[*]

Department of Physics, Tohoku University, Sendai 980-8578, Japan

Motohiko Kusakabe[†]

School of Liberal Arts and Science, Korea Aerospace University, Goyang 412-791, Korea
and Department of Physics, Soongsil University, Seoul 156-743, Korea

Hiroshi Okada[‡]

School of Physics, KIAS, Seoul 130-722, Korea

The primordial lithium abundance inferred from spectroscopic observations of metal-poor stars is ~ 3 times smaller than the theoretical prediction in the standard big bang nucleosynthesis (BBN) model. We assume a simple model composed of standard model particles and a sterile neutrino ν_H with mass of $\mathcal{O}(10)$ MeV which decays long after BBN. We then investigate cosmological effects of a sterile neutrino decay, and check if a sterile neutrino can reduce the primordial lithium abundance. We formulate the injection spectrum of nonthermal photon induced by the ν_H decay. We take into account the generation of electrons and positrons, $e^{\pm}$'s, and active neutrinos at the ν_H decay, the primary photon production via the inverse Compton scattering of cosmic background radiation (CBR) by energetic $e^{\pm}$, and electromagnetic cascade showers induced by the primary photons. The steady state injection spectrum is then derived as a function of the ν_H mass and the photon temperature. The ν_H decay produces energetic active neutrinos which are not thermalized, and $e^{\pm}$'s which are thermalized. We then derive formulas relevant to the ν_H decay rates and formulas for the baryon-to-photon ratio η and effective neutrino number N_{eff}. The initial abundance, mass, and lifetime of ν are taken as free parameters. We then consistently solve (1) the cosmic thermal history, (2) nonthermal nucleosynthesis induced by the nonthermal photons, (3) the η value, and (4) the N_{eff} value. We find that an effective ^{7}Be destruction can occur only if the sterile neutrino decays at photon temperature $T = \mathcal{O}(1)$ keV. Amounts of energy injection at the ν_H decay are constrained from limits on primordial D and ^{7}Li abundances, the N_{eff} value, and the CBR energy spectrum. We find that ^{7}Be is photodisintegrated and the Li problem is partially solved for the lifetime 10^4–10^5 s and the mass $\gtrsim 14$ MeV. ^{7}Be destruction by more than a factor of 3 is not possible because of an associated D overdestruction. In the parameter region, the η value is decreased slightly, while the N_{eff} value is increased by a factor of $\Delta N_{\text{eff}} \lesssim 1$. In this study, errors in photodisintegration cross sections of ^{7}Be$(\gamma, \alpha)^3$He and ^{7}Li$(\gamma, \alpha)^3$H that have propagated through the literature are corrected, and new functions are derived based on recent nuclear experiments. It is found that the new photodisintegration rates are 2.3 to 2.5 times smaller than the old rates. The correct cross sections thus indicate significantly smaller efficiencies of ^{7}Be and ^{7}Li photodisintegration. Abundances of sterile neutrino necessary for the ^{7}Li reduction are much smaller than thermal freeze-out abundances. The relic sterile neutrino, therefore, must be diluted between the freeze-out and BBN epochs by some mechanism.

I. INTRODUCTION

The big bang nucleosynthesis (BBN) model [1] successfully explains primordial light element abundances inferred from astronomical observations (e.g., [2,3]) if the cosmological baryon density determined from the power spectrum of cosmic microwave background (CMB) radiation

measured with the Wilkinson Microwave Anisotropy Probe (WMAP) [4–7] or Planck [8] is adopted. An apparent discrepancy, however, exists between observational and theoretical ^{7}Li abundances. Spectroscopic observations of metal-poor stars (MPSs) indicate a plateau for the abundance ratio, ^{7}Li$/$H $= (1 - 2) \times 10^{-10}$, with small error bars as a function of metallicity for [Fe$/$H] > -3 [9] in the Galaxy [10–22] and ω Centauri accreted by the Galaxy [23] [24]. The plateau abundance is $\sim$3–4 times smaller than that predicted in the standard BBN (SBBN) model (e.g., ^{7}Li$/$H $= 5.24 \times 10^{-10}$ [2]; see Ref. [3] for theoretical light

[*]h_ishida@tuhep.phys.tohoku.ac.jp
[†]motohiko@kau.ac.kr
[‡]hokada@kias.re.kr

element abundances for the baryon density from Planck [8]). Recent observations also indicate a break of this plateau shown as small Li abundances with a large dispersion at lower metallicities of [Fe/H] < −3 [14,16–18,22,26,27]. Therefore, it seems that we need a mechanism for a metallicity-independent depletion from the primordial abundance to the plateau abundance and also another for a metallicity-dependent depletion from the plateau abundance. In this paper, we focus on the former universal depletion by cosmological processes. This Li problem (see Ref. [28] for a review) shows that some physical processes have reduced the primordial Li abundance in some epoch during or after BBN.

The standard stellar model suggests very small depletions of Li isotopes in surfaces of MPSs [29]. The ^{7}Li/H abundances of MPSs observed today are then approximately interstellar abundances when the MPSs formed. Nonstandard processes such as the rotationally induced mixing [30,31] and the turbulent mixing [32–34] have been suggested to reduce the ^{7}Li abundance in stellar atmospheres. In the former model, a large depletion factor does not realize simultaneously with a small dispersion in stellar Li abundances after the depletion. The depletion factor is then constrained to be small. In the latter model, a depletion of a factor of 1.6–2.0 [32] is predicted, although it is still unclear if this mechanism can deplete Li abundances of all MPSs rather uniformly.

Nonstandard BBN, on the other hand, may be responsible for the Li problem at least partially. We note that ^{7}Be is produced more than ^{7}Li in the SBBN model with the Planck baryon density. The ^{7}Be nuclei are then converted to ^{7}Li nuclei via recombination with electrons followed by the electron capture, i.e., ^{7}Be + e$^-$ → ^{7}Li + ν_e. Therefore, the Li problem is alleviated if some exotic processes could destroy ^{7}Be. One of the solutions to the Li problem is an injection of a nonthermal photon with energy of ∼2 MeV which can destroy ^{7}Be but not deuterium (D) as calculated in Ref. [35]. If a long-lived exotic particle radiatively decays after BBN, nonthermal photons can disintegrate background thermal nuclei, and light element abundances change [36]. If the energy of the photon emitted at the decay is much larger than $\mathcal{O}(10)$ MeV, all types of light nuclei are disintegrated by nonthermal photons [36–48]. In this case, therefore, the Li problem cannot be solved (e.g., [46,48]). Therefore, the energy of emitted photons for the ^{7}Be destruction is limited to a narrow range [35]. A similar ^{7}Be destruction would occur if a long-lived sterile neutrino decays into an energetic electron and positron. We then study the cosmological effects of this decay channel in this paper.

From the theoretical point of view of the extended minimal Standard Model (MSM) of particle physics, right-handed neutrinos introduced as sterile neutrinos provide an elegant mechanism for the generation of tiny active neutrino masses, the so-called canonical seesaw

mechanism [49–52]. If their masses are so large (more than 10^9 GeV), they also explain the origin of the baryon asymmetry of the Universe, the so-called leptogenesis scenario [53]. Even if the sterile neutrinos have masses below the electroweak (EW) scale, however, there exist other phenomenological effects without lacking the success of the seesaw mechanism. Several possibilities have been investigated regarding the detectability of the sterile neutrinos, and the case in which sterile neutrinos are lighter than light mesons (e.g., pion or kaon) has been studied especially in detail [54] (for a recent study, see [55] and references therein). The allowed sterile neutrino masses are smaller than the pion mass ∼140 MeV, which are not consistent with the recent results of neutrino oscillation experiments, unless one assumes that their lifetimes are longer than ∼0.1 s. In addition, another constraint has been derived from a study of BBN by a comparison between theoretical and observational abundances of ^{4}He. The upper limit on the lifetime of ∼0.1 s was derived when a relic abundance of sterile neutrino is fixed as given in Refs. [56,57]. However, this constraint depends on the relic abundance. In this paper, we take into account the possibility that the abundance is smaller than the simple estimate [56,57]. In this case, a longer lifetime of the sterile neutrino is allowed.

In this paper, we comprehensively investigate cosmological effects of a long-lived sterile neutrino with mass ∼10 MeV. In Sec. II, we assume a decay of a sterile neutrino in the early Universe, and we describe our calculation method and formulations of (1) the spectra of electrons and positrons generated at the decay, (2) those of primary photons induced by the energetic electrons and positrons, and (3) the nonthermal nucleosynthesis triggered by the energetic photons. In Sec. III, revised cross sections for photodisintegration of ^{7}Be and ^{7}Li are described. In Sec. IV, effects of the decaying sterile neutrino on the cosmic thermal history, the effective neutrino number, and the baryon-to-photon ratio are formulated. In Sec. V, observational constraints on primordial light element abundances, the effective neutrino number, and the baryon-to-photon ratio adopted in this paper are summarized. In Sec. VI, we show calculated energy spectra of electrons and positrons emitted at the decay, energy spectra of photons produced via the inverse Compton scattering of background photons by the electrons and positrons, and photon injection spectra resulting from electromagnetic cascade showers. Time evolutions of light element abundances, the baryon-to-photon ratio, and thermal and nonthermal neutrino energy densities are then consistently calculated with nonthermal photodisintegrations of nuclei taken into account. An impact of revised cross sections of ^{7}Be and ^{7}Li photodisintegrations is also shown. In Sec. VII, we discuss the relic abundance of the sterile neutrino before its decay. We also comment on a possible dilution of the sterile neutrino in the early Universe, effects of the sterile

neutrino mixing to active neutrinos of different flavors, and experimental constraints from the pion decay and the supernova luminosity. In Sec. VIII, this study is summarized. In the Appendix, extensive formulas of the sterile neutrino decay are derived. We adopt natural units of $\hbar = c = k_B = 1$, where $\hbar$ is the reduced Planck constant, c is the speed of light, and k_B is the Boltzmann constant. We also adopt the notation of $A(a,b)B$ for a reaction $A + a \to b + B$.

II. MODEL

We simply include one right-handed (sterile) neutrino, ν_H, in the MSM and assume that it has a mass of $\mathcal{O}(10)$ MeV and a rather long lifetime $\sim \mathcal{O}(10^5)$ s. We consider effects of the decays of the $\mathcal{O}(10)$ MeV sterile neutrino on cosmological quantities, especially the ^{7}Li number abundance relative to hydrogen, i.e., ^{7}Li/H.

A. Method

We perform a BBN calculation. Kawano's BBN code [58,59] is utilized with default settings of the time steps in order to make the thermal nucleosynthesis calculation part as simple as possible. To calculated results, we added Sarkar's correction for ^{4}He abundances from explicit integration of weak rates, smaller time steps, Coulomb, radiative, and finite temperature corrections, and the correction for finite nucleon mass [60]. Reaction rates for light nuclei ($A \leq 10$) are updated with recommendations by JINA REACLIB Database V1.0 [61]. The neutron lifetime is set to be 880.0 ± 0.9 s from the weighted average value of the Particle Data Group [62]. We note that after the improved measurements [63–65], a few earlier measurements have been reanalyzed, and updated lifetimes are significantly shorter than the previous ones [62].

We adopt cosmological parameters reported from the analysis of the Planck Collaboration [8]. Central values for the base ΛCDM model (Planck + WP + highL + BAO) determined from the Planck 2013 data are taken: $H_0 = 67.3 \pm 1.2$ km s^{-1} Mpc^{-1}, $\Omega_\Lambda = 0.685^{+0.018}_{-0.016}$, $\Omega_m = 0.315^{+0.016}_{-0.018}$, and $\Omega_b h^2 = 0.02205 \pm 0.00028$ with $h = H_0/(100$ km s^{-1} Mpc^{-1}). The baryon-to-photon ratio is calculated using the most recent values of physical constants as follows.

1. Baryon-to-photon ratio

The present number density of CMB is given by

$$n_{\gamma 0} = \frac{2\zeta(3)}{\pi^2} T_{\gamma 0}^3, \qquad (2.1)$$

where $\zeta(3) = 1.20205$ is the Riemann zeta function, and $T_{\gamma 0}$ is the present CMB temperature. The present energy density of baryons is related to cosmological parameters as

$$\rho_{b0} = \Omega_b \left(\frac{3H_0^2}{8\pi G_N} \right), \qquad (2.2)$$

where G_N is the gravitational constant. The present average mass per baryon is given [66] by

$$m_{b0} \equiv \frac{\rho_{b0}}{n_{b0}} = \left\{ 1 - \left[1 - \frac{1}{4} \left(\frac{m_{He}}{m_H} \right) Y_p \right] \right\} m_H$$
$$= (1 - 0.007119 Y_p) m_H, \qquad (2.3)$$

where n_{b0} is the present number density of baryons; $m_H = 1.67353 \times 10^{-21}$ and $m_{He} = 6.64648 \times 10^{-21}$ kg are the atomic masses of ^{1}H and ^{4}He, respectively [67]; and Y_p is the cosmological mass fraction of ^{4}He. In the above equation, contributions from small abundances of D, ^{3}He, ^{7}Li, and heavier nuclides have been neglected.

Using the above three equations, the relation between the baryon-to-photon ratio and the baryon density parameter is given [66] by

$$\frac{\eta}{\Omega_b h^2} = \frac{n_{b0}}{n_{\gamma 0}} \left[\frac{3(100 \text{ km s}^{-1} \text{ Mpc}^{-1})^2}{8\pi G_N m_H} \right] \frac{m_H}{\rho_{b0}}$$
$$= \frac{1}{n_{\gamma 0}} \left[\frac{3(100 \text{ km s}^{-1} \text{ Mpc}^{-1})^2}{8\pi G_N m_H} \right] \frac{m_H}{m_{b0}}$$
$$= 2.7378 \times 10^{-8} \left(\frac{G_N}{6.6738 \times 10^{-11} \text{ m}^3 \text{ kg}^{-1} \text{ s}^{-2}} \right)^{-1}$$
$$\times \left(\frac{T_{\gamma 0}}{2.7255 \text{ K}} \right)^{-3} [1 + 0.007131(Y_p - 0.25)].$$
$$(2.4)$$

We adopt the CMB temperature [68]

$$T_{\gamma 0} = 2.72548 \pm 0.00057 \text{ K}$$
$$= 2.72548(1 \pm 0.00021) \text{ K} \, (1\sigma). \qquad (2.5)$$

The latest gravitational constant [62] is given by

$$G_N = (6.67384 \pm 0.00080) \times 10^{-11} \text{ m}^3 \text{ kg}^{-1} \text{ s}^{-2}$$
$$= 6.67384(1 \pm 0.00012) \times 10^{-11} \text{ m}^3 \text{ kg}^{-1} \text{ s}^{-2} \, (1\sigma).$$
$$(2.6)$$

The square root of sum of squares of uncertainties from G_N and T_γ is taken, and the precise relation between η and $\Omega_b h^2$ is derived, for $Y_p \sim 0.25$, as

$$\eta = (6.037 \pm 0.077) \times 10^{-10} \, (1\sigma). \qquad (2.7)$$

2. Parameters

It is assumed that energetic electrons and positrons are generated at the decay of a long-lived massive particle

(sterile neutrino) ν_H. The sterile neutrino ν_H has a mass M_{ν_H} and a mean lifetime τ_{ν_H}. Through the inverse Compton scattering of cosmic background radiation (CBR), the energetic electrons and positrons produce energetic primary photons. The energies of the photons are related to the energy of $e^\pm$ and temperature of the Universe.

The present model has three parameters regarding effects of nonthermal nucleosynthesis: (1) $(n^0_{\nu_H}/n^0_\gamma)$ is the number ratio of the decaying particle ν_H and the background photon evaluated at a time between the cosmological electron-positron pair annihilation and the ν_H decay, (2) the ν_H mass M_{ν_H}, and (3) the lifetime τ_{ν_H}. The total energy of $e^\pm$ emitted at one ν_H decay event $E_{\nu_H \to e}$ is derived as a function of M_{ν_H}. This quantity is equivalent to the energy injected in the form of electromagnetic cascade showers. We adopt the method of Ref. [48] to calculate the nonthermal nucleosynthesis, where thermonuclear reactions are simultaneously solved. We utilized updated reaction rates of ^{4}He photodisintegration [Eqs. (2) and (3) of Ref. [69]] based on cross section data from measurements with laser-Compton photons [70,71]. In this work, we found errors in cross sections of reactions ^{7}Be$(\gamma, \alpha)^3$He and ^{7}Li$(\gamma, \alpha)^3$H [44] adopted in previous studies on the BBN model with the long-lived decaying particle. The errors are corrected in this calculation, as explained in Sec. VI.

B. Injection spectrum of photon

The injection spectrum of the nonthermal photon is given by

$$
p_\gamma(E_\gamma; T, M_{\nu_H}) = \frac{1}{\Gamma} \int_{m_e}^{M_{\nu_H}/2} \frac{d\Gamma}{dE_e}(M_{\nu_H}) dE_e
$$
$$
\times \int_0^{E_{\gamma0,\max}} P_{iC}(E_e, E_{\gamma0}; T)
$$
$$
\times p_{\gamma,EC}(E_\gamma, E_{\gamma0}; T) dE_{\gamma0}, \qquad (2.8)
$$

where T is the photon temperature of the Universe, m_e is the electron mass, $(1/\Gamma)d\Gamma/dE_e(M_{\nu_H})$ is the differential decay rate as a function of energy of $e^\pm$ and M_{ν_H} [cf. Eq. (A21)], $P_{iC}(E_e, E_{\gamma0}; T)$ is the energy spectrum of the primary photon ($E_{\gamma0}$) produced at inverse Compton scatterings of $e^\pm$ with energy E_e at temperature T, $p_{\gamma,EC}(E_\gamma, E_{\gamma0}; T)$ is the energy spectrum of the nonthermal photon with energy E_γ which is produced in the electromagnetic cascade showers triggered by the primary photon with energy $E_{\gamma0}$ at T, and $E_{\gamma0,\max}(E_e, T)$ is the maximum value of $E_{\gamma0}$ [Eq. (2.14)].

C. Sterile neutrino decay

Throughout this paper, we concentrate on the Dirac neutrino case. We denote the mass of the heaviest state of neutrinos as M_{ν_H} and the active-sterile mixing angle as Θ.

The energy spectrum of $e^\pm$, i.e., $d\Gamma/dE_e$ is calculated (Appendix) and input in Eq. (2.8). In this paper, we fix

parameters of the sterile neutrino as one possible simple example case as follows. The sterile neutrino couples to charged and neutral currents of the electron flavor only. The strengths of the ν_H coupling to the currents are given by Θ (for the electron) and 0 (for the muon and tauon).

We note that the investigation in this paper can be easily extended to the Majorana case. The only difference between the two cases is that decay rates of a Majorana sterile neutrino are twice as large as those of a Dirac neutrino when those neutrinos have the same parameter values of M_{ν_H} and Θ. The relevant Lagrangian of the neutrino sector including one Majorana sterile neutrino is given by

$$
\mathcal{L} = \bar{\nu}_H \gamma_\mu \partial^\mu \nu_H - F_\alpha \bar{L}_\alpha H \nu_H - \frac{M_{\nu_H}}{2} \bar{\nu}_H^C \nu_H + \text{H.c.}, \qquad (2.9)
$$

where L_α and H are lepton and Higgs doublets, respectively; F_α (for $\alpha = e, \mu, \tau$) is the Yukawa coupling constant; and M_{ν_H} is the Majorana mass. After the breaking of EW symmetry, the sterile neutrino is mixed with active neutrinos. The degree of mixing is characterized by the active-sterile mixing denoted as $\Theta \equiv F_\alpha \langle H \rangle / M_{\nu_H}$, where $\langle H \rangle$ denotes the vacuum expectation value of the Higgs field.

The sterile neutrino can decay through this mixing into 3ν or $\nu\ell^+\ell^-$, where ℓ is a charged lepton species. Inversely, if the sterile neutrino is relatively light, it can be produced by the decay of light mesons. For instance when $M_{\nu_H} < m_\pi$ (pion mass) is satisfied, the pion decay can produce the sterile neutrino. In this case, we can find a signal of the sterile neutrino as a new peak in the energy spectrum of active neutrinos.

D. Primary photon spectrum

We assume that energetic electrons and positrons, $e^\pm$'s, are injected at the ν_H decay. Energetic photons, γ's, are then produced via the inverse-Compton scattering between the $e^\pm$'s and CBR ($e^\pm + \gamma_{bg} \to e^\pm + \gamma$), where the subscript "bg" means background. The inverse-Compton process plays an important role in developments of electromagnetic cascade shower. It distributes the energy of $e^\pm$ generated at the decay to multiple particles, i.e., γ's and $e^\pm$'s in the thermal bath. We assume that the $e^\pm$ in the initial state with energy E_e reacts with CBR with energy $E_{\gamma b}$, and a scattered photon in the final state has energy $E_{\gamma0}$. The number of collisions for an $e^\pm$ particle per unit time dt and unit energy interval of photon in the final state $dE_{\gamma0}$ is then approximately given [41,72] [73] by

$$
\frac{d^2N}{dt dE_{\gamma0}} = \frac{2\pi r_e^2 m_e^2}{E_{\gamma b} E_e^2} F(E_{\gamma0}, E_e; E_{\gamma b}), \qquad (2.10)
$$

where $r_e = \alpha/m_e$ is the classical radius of the electron with the fine structure constant α, and the function $F(E_{\gamma0}, E_e; E_{\gamma b})$ is defined by

$$F(E_{\gamma 0}, E_e; E_{\gamma b}) = \begin{cases} 2q \ln q + (1 + 2q)(1 - q) + \frac{(\gamma_E q)^2}{2(1 + \gamma_E q)}(1 - q) & \text{for } 0 < q \leq 1, \\ 0 & \text{otherwise,} \end{cases} \qquad (2.11)$$

where parameters are introduced as

$$\gamma_E = \frac{4 E_{\gamma b} E_e}{m_e^2}, \qquad q = \frac{E_{\gamma 0}}{\gamma_E (E_e - E_{\gamma 0})}. \qquad (2.12)$$

The energy spectrum of CBR in the early Universe is almost completely described by a Planck distribution,

$$f_{\gamma b}(E_{\gamma b}) = \frac{E_{\gamma b}^2}{\pi^2} \frac{1}{\exp(E_{\gamma b}/T) - 1}. \qquad (2.13)$$

The energy of the photon in the final state has an upper limit [72],

$$E_{\gamma 0} \leq E_{\gamma 0,\max} = \frac{4 E_{\gamma b} E_e^2}{m_e^2 (1 + 4 E_{\gamma b} E_e / m_e^2)}. \qquad (2.14)$$

When the maximum photon energy is between the threshold energies for the photodisintegration of ^{7}Be (1.59 MeV) and that of D (2.22 MeV), an effective destruction of ^{7}Be is

possible without destructions of other light nuclides [35]. The maximum energy should, therefore, be in this energy range, i.e., $E_{\gamma 0,\max} \sim 2$ MeV. Here we approximately take the average energy of CBR, $\bar{E}_{\gamma b} = 2.701 T$, as the CBR energy. The $e^\pm$ energy required for the generation of a nonthermal photon with $E_{\gamma 0} \sim 2$ MeV is then estimated to be

$$E_e \gtrsim \frac{1}{2} \left(E_{\gamma 0,\max} + m_e \sqrt{\frac{E_{\gamma 0,\max}}{E_{\gamma b}}} \right)$$

$$\sim 7.5 \text{ MeV} \quad (\text{for } t = 10^6 \text{ s}). \qquad (2.15)$$

Generally, at inverse Compton scatterings of low energy CBRs by energetic $e^\pm$ in the early Universe, small fractions of energies of $e^\pm$ are transferred to those of CBRs at respective scatterings, i.e., $E_{\gamma 0} \lesssim E_e$. The energy spectrum of the primary photon produced at the inverse Compton scattering is, therefore, approximately proportional to the differential scattering rate as a function of $E_{\gamma 0}$. The spectrum of the primary photon is then given by

$$P_{\text{iC}}(E_e, E_{\gamma 0}; T) = \frac{F(E_{\gamma 0}, E_e; E_{\gamma b})}{\int F(E_{\gamma 0}, E_e; E_{\gamma b}) dE_{\gamma 0}} = \frac{F(E_{\gamma 0}, E_e; E_{\gamma b})}{\frac{E_e}{\gamma_E} \left[\frac{8 + 9\gamma_E + \gamma_E^2}{2\gamma_E} \ln(1 + \gamma_E) - \frac{16 + 18\gamma_E + \gamma_E^2}{4(1 + \gamma_E)} + 2\text{Li}_2(-\gamma_E) \right]}, \qquad (2.16)$$

where $\text{Li}_2(-x)$ is the dilogarithm. The dilogarithm is calculated in our code using the published Algorithm 490 [74].

E. Electromagnetic cascade

The energetic primary photons interact with the CBR, and electromagnetic cascade showers composed of energetic photons and $e^\pm$'s develop (e.g., [37,41]). One energetic photon can produce multiple particles of lower energies by continuous reactions of pair production at a collision with CBR ($\gamma + \gamma_{\text{bg}} \to e^+ + e^-$) and the inverse Compton scattering of $e^\pm$ at a collision with CBR ($e^\pm + \gamma_{\text{bg}} \to e^\pm + \gamma$). The nonthermal photons then obtain a quasistatic equilibrium spectrum [41,75].

When the energy of the primary photon $E_{\gamma 0}$ is much larger than the threshold energy for photodisintegration of light nuclides, i.e., $E_{\gamma 0} \gg 1$ MeV, the steady state energy spectrum of the nonthermal photons is approximately given (e.g., [44,48,76]) by

$$p_{\gamma,\text{EC}}(E_\gamma, E_{\gamma 0}; T) = \begin{cases} K(E_X/E_\gamma)^{3/2} & \text{for } E_\gamma \leq E_X, \\ K(E_X/E_\gamma)^2 & \text{for } E_X < E_\gamma \leq E_C, \\ 0 & \text{for } E_C < E_\gamma, \end{cases} \qquad (2.17)$$

where $E_X \sim m_e^2/(80T)$ and $E_C \sim m_e^2/(22T)$ [41] are the energy corresponding to a break in the power law and a cutoff energy, respectively; and $K = E_{\gamma 0}/\{E_X^2 [2 + \ln(E_C/E_X)]\}$ is the normalization constant which conserves the energy of the primary photon. If nonthermal photons have energies larger than E_C, they are quickly destroyed via the electron-positron pair production.

The maximum energy of the nonthermal photon $E_{\gamma 0}$, however, can be of the order of $\mathcal{O}(1$ MeV) depending on the mass M_{ν_H} and the temperature T [Eq. (2.14)]. In this case, the generalized photon spectrum is given [35] as follows:

(1) For $E_{\gamma 0} \leq E_X$, the spectrum is given by

$$p_{\gamma,\text{EC1}}(E_\gamma, E_{\gamma 0}; T)$$
$$= \begin{cases} K_1 (E_X/E_\gamma)^{3/2} & \text{for } E_\gamma \leq E_{\gamma 0}, \\ 0 & \text{for } E_{\gamma 0} < E_\gamma, \end{cases} \quad (2.18)$$

where $K_1 = E_{\gamma 0}^{1/2}/(2E_X^{3/2})$.

(2) For $E_X < E_{\gamma 0} \leq E_C$, the spectrum is given by

$$p_{\gamma,\text{EC2}}(E_\gamma, E_{\gamma 0}; T)$$
$$= \begin{cases} K_2 (E_X/E_\gamma)^{3/2} & \text{for } E_\gamma \leq E_X, \\ K_2 (E_X/E_\gamma)^2 & \text{for } E_X < E_\gamma \leq E_{\gamma 0}, \\ 0 & \text{for } E_{\gamma 0} < E_\gamma, \end{cases}$$
$$\quad (2.19)$$

where $K_2 = E_{\gamma 0}/\{E_X^2[2 + \ln(E_{\gamma 0}/E_X)]\}$.

(3) For $E_C < E_{\gamma 0}$, the spectrum $p_{\gamma,\text{EC3}}(E_\gamma, E_{\gamma 0}, T)$ is given by Eq. (2.17).

F. Steady state spectrum

Rates of electromagnetic interactions are faster than the cosmic expansion rate. The injection spectrum $p_\gamma(E_\gamma, T, M_{\nu_H})$ is then quickly modified to a new quasistatic equilibrium spectrum given by

$$\mathcal{N}_\gamma^{\text{QSE}}(E_\gamma; T, M_{\nu_H}, \tau_{\nu_H}, \zeta_{\nu_H \to e})$$
$$= \frac{n_{\nu_H}(T; M_{\nu_H}, \tau_{\nu_H}, \zeta_{\nu_H \to e}) p_\gamma(E_\gamma; T, M_{\nu_H})}{\Gamma_\gamma(E_\gamma; T, M_{\nu_H}, \tau_{\nu_H}, \zeta_{\nu_H \to e}) \tau_{\nu_H}}, \quad (2.20)$$

where

$$n_{\nu_H}(T; M_{\nu_H}, \tau_{\nu_H}, \zeta_{\nu_H \to e})$$
$$= n_{\nu_H}^0 (1+z)^3 \exp(-t(T; M_{\nu_H}, \tau_{\nu_H}, \zeta_{\nu_H \to e})/\tau_{\nu_H}) \quad (2.21)$$

is the number density of the decaying particles ν_H at a redshift z, and $\zeta_{\nu_H \to e} = (n_{\nu_H}^0/n_\gamma^0)E_{\nu_H \to e}$ is a parameter describing the amount of electromagnetic energy injection, with $n_{\nu_H}^0$ and n_γ^0 the comoving number densities of ν_H and CBR, respectively, estimated at a time between the cosmological $e^\pm$ annihilation and the ν_H decay. Here, the cosmic time is described as $t(T; M_{\nu_H}, \tau_{\nu_H}, \zeta_{\nu_H \to e})$ taking the inverse function of the temperature evolution $T(t; M_{\nu_H}, \tau_{\nu_H},$

$\zeta_{\nu_H \to e})$. The quantity Γ_γ is the energy degradation rate of the nonthermal photons through three relatively slow processes: Compton scattering $(\gamma + e_{\text{bg}}^\pm \to \gamma + e^\pm)$, Bethe-Heitler ordinary pair creation in nuclei $(\gamma + N_{\text{bg}} \to e^+ + e^- + N)$, and double photon scattering $(\gamma + \gamma_{\text{bg}} \to \gamma + \gamma)$, where N is a nucleon in the nucleus. Since the energy degradation rate depends not only on the photon temperature but also on the baryon and electron densities [41], it is a function of the baryon-to-photon ratio η. We fix the η value after the ν_H decay to the observed value from the Planck CBR measurement. The entropy production associated with the ν_H decay changes the η value as a function of time. Therefore, the time evolution of the baryon-to-photon ratio depends on the parameters, i.e., $\eta = \eta(T; M_{\nu_H}, \tau_{\nu_H}, \zeta_{\nu_H \to e})$. We use this steady state approximation for the nonthermal photon spectrum.

G. Nonthermal nucleosynthesis

If the injection of nonthermal photons occurs at a cosmic time $t \gtrsim 10^4$ s, the nonthermal photons can disintegrate background nuclei, and nuclear abundances can be changed [36–48,77].

1. Photodisintegration

The equation describing a time evolution of nuclear abundance by primary reactions, i.e., photodisintegration, is given by

$$\frac{dY_A}{dt} = \sum_P N_{AC}[P\gamma]_A Y_T - \sum_P [A\gamma]_P Y_A, \quad (2.22)$$

where $Y_i \equiv n_i/n_B$ is the mole fraction of a nuclear species i with n_i and n_B number densities of nuclide i and total baryon, respectively [78], and we define the reaction rate

$$[P\gamma]_A = \frac{\eta_{\nu_H}(T; M_{\nu_H}, \tau_{\nu_H}, \zeta_{\nu_H \to e}) E_{\nu_H \to e}}{\tau_{\nu_H}}$$
$$\times G_{[P\gamma]_A}^1(T; M_{\nu_H}, \tau_{\nu_H}, \zeta_{\nu_H \to e}), \quad (2.23)$$

where $\eta_{\nu_H} = n_{\nu_H}/n_\gamma$ is the ν_H-to-photon number ratio with n_γ the number density of CBR, and the nuclear transfer function and the normalized spectrum of nonthermal photons are defined as

$$G_{[P\gamma]_A}^1(T; M_{\nu_H}, \tau_{\nu_H}, \zeta_{\nu_H \to e}) = \int_0^\infty dE_\gamma T_\gamma^{\text{QSE}}(E_\gamma; T, M_{\nu_H}, \tau_{\nu_H}, \zeta_{\nu_H \to e})\sigma_{\gamma+P \to A}(E_\gamma), \quad (2.24)$$

and

$$T_\gamma^{\text{QSE}}(E_\gamma; T, M_{\nu_H}, \tau_{\nu_H}, \zeta_{\nu_H \to e}) = \frac{\tau_{\nu_H} n_\gamma(T)}{E_{\nu_H \to e} n_{\nu_H}(T; M_{\nu_H}, \tau_{\nu_H}, \zeta_{\nu_H \to e})} \mathcal{N}_\gamma^{\text{QSE}}(E_\gamma; T, M_{\nu_H}, \tau_{\nu_H}, \zeta_{\nu_H \to e})$$
$$= \frac{p_\gamma(E_\gamma, T, M_{\nu_H})}{E_{\nu_H \to e}[\Gamma_\gamma/n_\gamma](E_\gamma; T, M_{\nu_H}, \tau_{\nu_H}, \zeta_{\nu_H \to e})}. \quad (2.25)$$

The first and second terms on the right-hand side (rhs) in Eq. (2.22) correspond to the production ($\gamma + P \rightarrow A + C$) and destruction ($\gamma + A \rightarrow P + D$), respectively, for nuclide A. The cross section of the process $\gamma + P \rightarrow A + C$ is denoted by $\sigma_{\gamma + P \rightarrow A}(E_\gamma)$. In addition, we use N_{AC} as the number of identical nuclear species in a production process: $N_{AC} = 2$ when particles A and C are identical and $N_{AC} = 1$ when they are not. For example, in the process ${}^4\text{He}(\gamma, d)\text{D}$, $N_{\text{DD}} = 2$ since two deuterons are produced at one reaction.

2. Secondary process

Nonthermal nuclei produced in the primary reaction can in general experience secondary nonthermal nuclear reactions. We, however, focus on an injection of photons with relatively small energies generated by a light sterile neutrino of $M_{\nu_\text{H}} \leq 20$ MeV. In this case, ${}^4\text{He}$ photodisintegration is impossible, and most of the important

secondary reactions do not occur. In this calculation, only the secondary reactions ${}^7\text{Li}(\gamma, n){}^6\text{Li}(p, \alpha){}^3\text{He}$ and ${}^7\text{Be}(\gamma, p){}^6\text{Li}(p, \alpha){}^3\text{He}$ are operative. The equation describing the secondary production and destruction is given by

$$\frac{dY_S}{dt} = \sum_{P,A,P',X_1,X_2} Y_P Y_{P'} \frac{N_{AX_1} N_{SX_2}}{N_{AP'}} [P(A)P']_S$$
$$- (\text{destruction term}), \tag{2.26}$$

where the reaction rate for a secondary reaction $P(\gamma, X_1)A(P', X_2)S$ with any combination of particles X_1, A, and X_2 is given by

$$[P(A)P']_S = \frac{\eta_{\nu_\text{H}}(T; M_{\nu_\text{H}}, \tau_{\nu_\text{H}}, \zeta_{\nu_\text{H} \rightarrow e}) E_{\nu_\text{H} \rightarrow e}}{\tau_{\nu_\text{H}}}$$
$$\times G^2_{[P(A)P']_S}(T; M_{\nu_\text{H}}, \tau_{\nu_\text{H}}, \zeta_{\nu_\text{H} \rightarrow e}), \tag{2.27}$$

$$G^2_{[P(A)P']_S}(T; M_{\nu_\text{H}}, \tau_{\nu_\text{H}}, \zeta_{\nu_\text{H} \rightarrow e}) = \int_0^\infty dE_A \frac{\sigma_{A+P' \rightarrow S}(E_A)\beta_A(E_A)}{[b_A/n_b](E_A; T, M_{\nu_\text{H}}, \tau_{\nu_\text{H}}, \zeta_{\nu_\text{H} \rightarrow e})}$$
$$\times \int_{\mathcal{E}_A^{-1}(E_A)}^\infty dE_\gamma T_\gamma^{\text{QSE}}(E_\gamma; T, M_{\nu_\text{H}}, \tau_{\nu_\text{H}}, \zeta_{\nu_\text{H} \rightarrow e})\sigma_{\gamma + P \rightarrow A}(E_\gamma)$$
$$\times \exp\left[-\int_{E_A}^{\mathcal{E}_A(E_\gamma)} dE_A' \frac{\Gamma_A(E_A')}{b_A(E_A'; T, M_{\nu_\text{H}}, \tau_{\nu_\text{H}}, \zeta_{\nu_\text{H} \rightarrow e})} \right], \tag{2.28}$$

where β_A is the velocity of the nuclide produced in a primary reaction, i.e., primary nuclide, A; $b_A = -dE_A/dt$ is the energy loss rate of the primary nuclide mainly from Coulomb scattering of electrons; and Γ_A is the destruction rate of the primary nuclide. Stable nuclides have $\Gamma_A = 0$, while unstable nuclides have nonzero values given by the β-decay rates. The quantity $\mathcal{E}_A(E_\gamma)$ is the energy of the nuclide A produced at the reaction $\gamma + P \rightarrow A$ of a nonthermal photon with energy E_γ, and $\mathcal{E}_A^{-1}(E_A)$ is the energy of the nonthermal photon which produces the primary nuclide A with energy E_A.

The transfer functions $G^1_{[P\gamma]_A}(T; M_{\nu_\text{H}}, \tau_{\nu_\text{H}}, \zeta_{\nu_\text{H} \rightarrow e})$ and $G^2_{[P(A)P']_S}(T; M_{\nu_\text{H}}, \tau_{\nu_\text{H}}, \zeta_{\nu_\text{H} \rightarrow e})$ should be derived as a function of T for a fixed parameter set of $(M_{\nu_\text{H}}, \tau_{\nu_\text{H}}, \zeta_{\nu_\text{H} \rightarrow e})$. Time evolutions of the temperature $T(t)$, the baryon-to-photon ratio $\eta(t)$, and the ν_H-to-photon ratio $\eta_{\nu_\text{H}}(t) = n_{\nu_\text{H}}/n_\gamma$ are different for different parameter sets. In Eq. (2.24), the parameter dependence of the transfer function comes from the steady state nonthermal photon spectrum $p_\gamma(E_\gamma, T, M_{\nu_\text{H}})$ and the energy loss rate per background photon $[\Gamma_\gamma/n_\gamma](E_\gamma; T, M_{\nu_\text{H}}, \tau_{\nu_\text{H}}, \zeta_{\nu_\text{H} \rightarrow e})$. In Eq. (2.28), b_A/n_b is independent of the baryon-to-photon ratio η at the time since the energy loss rate of the energetic nuclide, b_A, is proportional to the baryon density [79]. However, it depends on the η value at BBN through the ${}^4\text{He}$

abundance (or the electron abundance). Then, the quantity b_A/n_b, the photon spectrum T_γ^{QSE}, and the energy loss rate b_A in the exponential term depend on the parameter set $(M_{\nu_\text{H}}, \tau_{\nu_\text{H}}, \zeta_{\nu_\text{H} \rightarrow e})$.

3. Approximation

In this study, we calculate the transfer functions neglecting the entropy production by the sterile neutrino decay. Then, the η value is constant and set to be consistent with the central value determined by Planck. Also, the ν_H-to-photon ratio is exactly described as $\eta_{\nu_\text{H}} = (n_{\nu_\text{H}}^0/n_\gamma^0) \exp(-t/\tau_{\nu_\text{H}})$ [cf. Eq. (2.21)]. In this case, the transfer functions depend on the temperature T and the mass M_{ν_H} only. The reaction rates [Eqs. (2.23) and (2.27)] then reduce to

$$[P\gamma]_A = \frac{\zeta_{\nu_\text{H} \rightarrow e}}{\tau_{\nu_\text{H}}} \exp(-t/\tau_{\nu_\text{H}}) G^1_{[P\gamma]_A}(T; M_{\nu_\text{H}}), \tag{2.29}$$

$$[P(A)P']_S = \frac{\zeta_{\nu_\text{H} \rightarrow e}}{\tau_{\nu_\text{H}}} \exp(-t/\tau_{\nu_\text{H}}) G^2_{[P(A)P']_S}(T; M_{\nu_\text{H}}). \tag{2.30}$$

We calculate nonthermal nucleosynthesis triggered by the nonthermal photons taking τ_{ν_H}, $\zeta_{\nu_\text{H} \rightarrow e}$, and M_{ν_H} as parameters. By using these simplified transfer functions, a

parameter search can be performed with same transfer functions for respective M_{ν_H} values in realistic computation time.

We can safely use the simplified transfer functions without missing a parameter region in which the primordial ^{7}Li abundance is reduced for the following reason. In this model, the entropy production by the ν_H decay always reduces the baryon-to-photon ratio as a function of time (Sec. IV). The ratio in the BBN epoch is, therefore, larger than that in the cosmological recombination epoch measured by Planck. Then, one can place a lower limit on the BBN η value taking the Planck value. On the other hand, deuterium is only destroyed by photodisintegration, and is never produced in the nonthermal nucleosynthesis by the ν_H decay. The abundance of deuterium produced at the BBN, therefore, cannot be significantly smaller than the observational constraint on the primordial abundance. This requirement gives an upper limit on the BBN η value since primordial D abundance decreases as a function of η. These limits are satisfied in a very narrow region of the BBN η value, only $\mathcal{O}(1)\%$ wide, which is around the Planck value (see Fig. 1 of Ref. [80] or Fig. 1 of Ref. [3]). Then, maximum allowed changes of the η value between the BBN and the recombination epochs is $\mathcal{O}(1)\%$. Also the η_{ν_H} value in the case with an entropy production can change from that in the case without it by only $\mathcal{O}(1)\%$. The neglect of the entropy production effect in Eqs. (2.29) and (2.30), therefore, does not introduce a large error in final nuclear abundances. In the following calculation, the final η value is fixed to the Planck value. When the entropy production changes the η and η_{ν_H} values by more than $\sim 10\%$, present
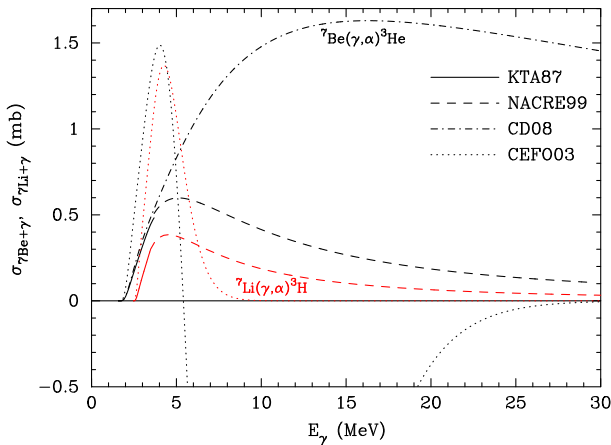
results of the nonthermal nucleosynthesis calculation are not precise. However, such a large entropy production is accompanied by a large BBN η value and is therefore excluded by underproduction of deuterium definitely.

III. PHOTODISINTEGRATION CROSS SECTIONS OF ^{7}Be AND ^{7}Li

We correct significant errors in cross sections of reactions ^{7}Be$(\gamma, \alpha)^3$He and ^{7}Li$(\gamma, \alpha)^3$H [44] adopted in previous studies on the BBN model including a decaying particle (e.g., [35,48,69,77]).

The detailed balance relation between cross sections of a forward reaction $A(B, \gamma)C$ and its inverse reaction $C(\gamma, B)A$ is described [81] as

$$\sigma_{C+\gamma} = \frac{g_A g_B}{(1 + \delta_{AB}) g_C} \left(\frac{\mu E}{E_\gamma^2} \right) \sigma_{A+B}, \qquad (3.1)$$

where σ_{A+B} and $\sigma_{C+\gamma}$ are the forward and inverse reaction cross sections, respectively; $g_i = 2I_i + 1$ is the statistical degrees of freedom (d.o.f.'s) with spin I_i of species i; δ_{AB} is the Kronecker delta for avoiding the double counting of identical particles; μ and E are the reduced mass and the center of mass (CM) energy, respectively, of the $A + B$ system; and $E_\gamma = E + Q$ is the radiation energy with Q the reaction Q value: $Q = 1.586627$ MeV [for ^{3}He$(\alpha, \gamma)^7$Be] and $Q = 2.467032$ MeV [for ^{3}H$(\alpha, \gamma)^7$Li], respectively.

The forward reaction rate is described using the astrophysical S factor as

$$\sigma_{A+B} = \frac{S}{E} \exp \left(-\sqrt{\frac{E_G}{E}} \right), \qquad (3.2)$$

where $E_G = (2\mu)(\pi Z_A Z_B \alpha)^2$ is the Gamow energy with Z_i the proton number of species i and $\alpha = 1/137.04$ the fine structure constant. Inserting this equation in Eq. (3.1), we obtain a relation between the cross section of the inverse (photodisintegration) reaction and the S factor of the forward (radiative capture) reaction:

$$\sigma_{C+\gamma} = \frac{g_A g_B}{(1 + \delta_{AB}) g_C} \left(\frac{\mu}{E_\gamma^2} \right) S \exp \left(-\sqrt{\frac{E_G}{E}} \right). \qquad (3.3)$$

Firstly, S factors of the two reactions are taken from Ref. [82]. When we take fitted functions [their Eqs. (6) and (7)] with theoretical values of $S(0) = 0.511$ keV b for ^{7}Be$(\gamma, \alpha)^3$He and $S(0) = 0.1003$ keV b for ^{7}Li$(\gamma, \alpha)^3$H, the photodisintegration cross sections are given by

$$\sigma_{^7\text{Be}+\gamma} = \frac{409 \text{ mb}}{E_{\gamma,\text{MeV}}^2} \exp \left(-\frac{5.19}{E_{\text{MeV}}^{1/2}} \right) \exp(-0.548 E_{\text{MeV}})$$
$$\times (1 - 0.4285 E_{\text{MeV}}^2 + 0.5340 E_{\text{MeV}}^3 - 0.1150 E_{\text{MeV}}^4)$$
$$(\text{for } Q \leq E_\gamma \leq Q + 2.1 \text{ MeV}), \qquad (3.4)$$

FIG. 1 (color online). Cross sections of reactions ^{7}Be$(\gamma, \alpha)^3$He and ^{7}Li$(\gamma, \alpha)^3$H as a function of the photon energy. They are estimated from the detailed balance relation with the forward radiative capture cross sections. Solid lines correspond to polynomial fits to theoretical calculations in the low energy regions [82]. Dashed lines correspond to constant S factors in the high energy regions [83]. The dot-dashed line is from a fit to experimental data on ^{3}He$(\gamma, \alpha)^7$Be [92]. Dotted lines show fitted functions of Ref. [44].

where $E_{\gamma,\mathrm{MeV}} = E_\gamma/\mathrm{MeV}$ and $E_{\mathrm{MeV}} = E/\mathrm{MeV}$ are defined, and

$$\sigma_{^7\mathrm{Li}+\gamma} = \frac{80.3\text{ mb}}{E_{\gamma,\mathrm{MeV}}^2} \exp\left(-\frac{2.60}{E_{\mathrm{MeV}}^{1/2}}\right) \exp(-2.056 E_{\mathrm{MeV}})$$
$$\times (1 + 2.2875 E_{\mathrm{MeV}}^2 - 1.1798 E_{\mathrm{MeV}}^3 + 2.5279 E_{\mathrm{MeV}}^4)$$
$$(\text{for } Q \le E_\gamma \le Q + 1\text{ MeV}). \qquad (3.5)$$

It is found that both cross sections are smaller than the published values [44] by a factor of about 3 although the values were based on the same reference [82]. It is expected that this error originates from the wrong treatment of the statistical d.o.f.

Another error stems from the use of the fitted functions [82] which can be reasonably applied only to the low energy region of $E_\gamma - Q \lesssim \mathcal{O}(1)$ MeV. The functions have been derived from fitting to measured data in a relatively low energy region. These functions then provide erroneous values in a large E_γ region. In particular, the function for $^7\mathrm{Be}(\gamma,\alpha)^3\mathrm{He}$ outputs large negative values at $E_\gamma \gtrsim 5.4$ MeV. Since this error affects the final nuclear abundances calculated in the model with a decaying particle, it must be fixed. For example, we may assume constant S factors: $S = 0.31$ keV b at $E_\gamma > Q + 2.1$ MeV for $^7\mathrm{Be}(\gamma,\alpha)^3\mathrm{He}$ and $S = 0.06$ keV b at $E_\gamma > Q + 1$ MeV for $^7\mathrm{Li}(\gamma,\alpha)^3\mathrm{H}$ (cf. Ref. [83]). The cross sections are then given by

$$\sigma_{^7\mathrm{Be}+\gamma} = \frac{248\text{ mb}}{E_{\gamma,\mathrm{MeV}}^2} \exp\left(-\frac{5.19}{E_{\mathrm{MeV}}^{1/2}}\right) \quad \text{for } Q + 2.1\text{ MeV} \le E_\gamma,$$
$$(3.6)$$

$$\sigma_{^7\mathrm{Li}+\gamma} = \frac{48.1\text{ mb}}{E_{\gamma,\mathrm{MeV}}^2} \exp\left(-\frac{2.60}{E_{\mathrm{MeV}}^{1/2}}\right) \quad \text{for } Q + 1\text{ MeV} \le E_\gamma.$$
$$(3.7)$$

Recently, three independent groups have measured the cross section of the reaction $^3\mathrm{He}(\alpha,\gamma)^7\mathrm{Be}$ at high energies ($E \gtrsim 1.5$ MeV) with relatively small errors [84–87]. There is only one earlier publication for the cross section measured in this energy region, and the measured data included large errors [88]. The new measurements indicated a possible increase of the cross section at $E \gtrsim 1.5$ MeV which was not seen in the earlier work. Theoretically, this increase can be understood as a contribution of the electric dipole capture from the scattering d-wave which gradually becomes more important at higher energies [89,90]. When we consider these experimental results, it may be better to take into account the d-wave behavior in an estimation of the cross section at high energies rather than to assume a constant S factor. We note, however, that a precise estimation needs more measurements at high energy of $E > 3$ MeV. The only

experimental data in the high energy region are from measurements for the $^3\mathrm{He}$ incident energy $E_3 = 19$–26 MeV at the angle $90°$ [91]. The measured data typically give only upper limits on the differential cross section, $d\sigma/d\Omega(90°) \lesssim 1\ \mu\mathrm{b/sr}$, at the corresponding CM energy $E \sim 12$–17 MeV.

An analytical function has been fitted to cross sections measured between 2004 and 2007 in the energy range of $0.04 \le E \le 1.2$ MeV [92]. Although this fitting did not take into account experimental data at higher energies, dominant contributions of s- and d-waves are included in the analytical function. We then adopt this cross section function with six parameters in this paper. The photodisintegration cross section is given by

$$\sigma_{^7\mathrm{Be}+\gamma} = \frac{801\text{ mb}}{E_{\gamma,\mathrm{MeV}}^2} \exp\left(-\frac{5.19}{E_{\mathrm{MeV}}^{1/2}}\right) \sum_{i=0,1} \frac{Q_i}{E + Q_i}$$
$$\times \left[s_{0i}(1 + a_i E_{\mathrm{MeV}})^2 + s_{2i}\left(1 + 4\pi^2 \frac{E}{E_\mathrm{G}}\right)\right.$$
$$\left. \times \left(1 + 16\pi^2 \frac{E}{E_\mathrm{G}}\right)\right], \qquad (3.8)$$

where $i = 0$ and 1 indicate capture cross sections to the ground and the first excited states of $^7\mathrm{Be}$, respectively, and $Q_0 = Q$ and $Q_1 = 1.1570$ MeV are the Q values for the two final states. The six fitted parameters are $s_{00} = 0.406$, $s_{20} = 0.007$, $a_0 = -0.207$, $s_{01} = 0.163$, $s_{21} = 0.004$, and $a_1 = -0.134$.

Figure 1 shows cross sections of reactions $^7\mathrm{Be}(\gamma,\alpha)^3\mathrm{He}$ and $^7\mathrm{Li}(\gamma,\alpha)^3\mathrm{H}$ as a function of the photon energy. The cross sections are derived by applying the detailed balance relation to the forward radiative capture cross sections. Solid and dashed lines correspond to polynomial fits to theoretical calculations in low energy regions [82] and constant S factors in high energy regions [83], respectively. The dot-dashed line corresponds to a fit to experimental data on $^3\mathrm{He}(\gamma,\alpha)^7\mathrm{Be}$ [92]. For comparison, dotted lines show fitted functions of Ref. [44]. We adopt the dot-dashed line [Eq. (3.8)] for $^7\mathrm{Be}(\gamma,\alpha)^3\mathrm{He}$, and the solid and the dashed lines [Eqs. (3.5) and (3.7)] for $^7\mathrm{Li}(\gamma,\alpha)^3\mathrm{H}$ in the following calculations.

IV. EFFECTS ON COSMIC PHOTON AND NEUTRINO BACKGROUND

The decay of sterile neutrinos has two effects on the resulting effective neutrino number in the Universe, i.e., N_{eff}. Firstly, since the decay generates energetic neutrinos, the total energy density of neutrinos increases with respect to the case of no neutrino injection [93,94]. Secondly, since the decay also generates energetic electrons and positrons, the energy density of background photons increases [93–95]. The ratio between energy densities of neutrinos and photons is reduced, and as a result, the effective

neutrino number is reduced compared to the case of no photon injection. The baryon-to-photon ratio is simultaneously reduced by this photon heating effect. In this study, we assume that the lifetime of the sterile neutrino is much longer than the time scale of the decoupling of the active neutrino in the early Universe, i.e., $\tau_{\nu_H} \gg 1$ s. The energetic neutrino generated at the decay cannot interact effectively with background particles mainly constituted of weakly interacting neutrinos and weakly noninteracting photons. The energetic neutrino is then never thermalized and propagates in the Universe without collisions.

A. Cosmic thermal history

The total energy density in the Universe is given [93] by

$$\rho = \rho_\gamma + (\rho_{e^-} + \rho_{e^+}) + \rho_{\nu,\text{th}} + \rho_b + \rho_{\nu_H} + \rho_{\nu,\text{nt}}, \quad (4.1)$$

where ρ_i is the energy density of particle species $i = \gamma$ (photon), e^- (electron), e^+ (positron), ν,th (thermal neutrino), b (baryon), ν_H (sterile neutrino), and ν,nt (nonthermal neutrino produced at the ν_H decay). The last two terms are not present unless the decaying sterile neutrino exists. The sterile neutrino energy density is given [93] by

$$
\begin{aligned}
\rho_{\nu_H} &= M_{\nu_H} n_{\nu_H} \\
&= M_{\nu_H} n_{\nu_H}^0 (1+z)^3 \exp\left(-t/\tau_{\nu_H}\right) \\
&= M_{\nu_H} n_{\nu_H,\text{i}} \left(\frac{n_b}{n_{b,\text{i}}}\right) \exp\left(-t/\tau_{\nu_H}\right),
\end{aligned}
\quad (4.2)
$$

where n_i is the energy density of particle i, and $n_{i,\text{i}}$ is the energy density of i at time t_i ($t_i \gg 1$ MeV). The initial number density of ν_H is related as

$$n_{\nu_H,\text{i}} = \frac{11}{4} \frac{n_{\gamma,\text{i}} \zeta_{\nu_H \to e}}{E_{\nu_H \to e}}. \quad (4.3)$$

The factor $(11/4)$ originates from the entropy transfer from $e^\pm$'s to photons at the cosmological $e^\pm$ annihilation.

When the lifetime of the sterile neutrino is equal to or longer than the BBN time scale, the cosmic expansion rate can be affected by the energy density of the sterile neutrino. Since such a change in expansion rate changes resultant elemental abundances, it is constrained from observed light element abundances. For example, the energy density of exotic relativistic species in the BBN epoch has been constrained [96,97]. The sterile neutrino with a mass of $\mathcal{O}(10)$ MeV is nonrelativistic during BBN. The energy density of a nonrelativistic particle redshifts as a^{-3}, while that of a relativistic particle redshifts as a^{-4}. Therefore, the former increases relative to the latter as the Universe expands. The effect of the nonrelativistic sterile neutrino is thus different from that of the exotic relativistic particle. The change in the expansion rate during BBN is rigorously taken into account by using Eq. (4.1).

The nonthermal neutrino energy density is solved by time integration [93] of

$$\frac{d\rho_{\nu,\text{nt}}}{dt} = -4H\rho_{\nu,\text{nt}} + \frac{E_{\nu_H \to \nu}}{M_{\nu_H}} \frac{\rho_{\nu_H}}{\tau_{\nu_H}}, \quad (4.4)$$

where $E_{\nu_H \to \nu}$ is the average total energy of active neutrinos and antineutrinos emitted per one ν_H decay event, and the cosmic expansion rate is given by

$$H = \frac{\dot{a}}{a} = \left(\frac{8\pi G_N}{3}\rho\right)^{1/2}, \quad (4.5)$$

where a is the scale factor of the Universe. The integral form of Eq. (4.4) is given by

$$
\begin{aligned}
\rho_{\nu,\text{nt}}(t) &= \frac{\rho_{\nu_H,\text{i}} a_\text{i}^3}{a(t)^4} \frac{E_{\nu_H \to \nu}}{M_{\nu_H}} \frac{1}{\tau_{\nu_H}} \int_{t_\text{i}}^t a(t') e^{-t'/\tau_{\nu_H}} dt' \\
&= \left(\frac{11}{4}\right) n_{\gamma,\text{i}} \frac{E_{\nu_H \to e}}{\tau_{\nu_H}} \frac{E_{\nu_H \to \nu}}{E_{\nu_H \to e}} \frac{a_\text{i}^3}{a(t)^4} \int_{t_\text{i}}^t a(t') e^{-t'/\tau_{\nu_H}} dt',
\end{aligned}
\quad (4.6)
$$

where $\rho_{\nu_H,\text{i}} \approx M_{\nu_H} n_{\nu_H,\text{i}}$ is the initial energy density of ν_H, and a_i is the scale factor at time t_i. We used Eq. (4.3) at the second equality.

The ratio of the average total energy emitted in the form of electrons and positrons at the ν_H decay to the mass M_{ν_H} is given by

$$\frac{E_{\nu_H \to e}}{M_{\nu_H}} = \frac{1}{1 + R(\nu, e)}, \quad (4.7)$$

where $R(\nu, e)$ is the ratio of average total energies injected in the forms of ν (including all flavors and antineutrinos) and $e^\pm$ at the ν_H decay. In the present model, the sterile neutrino has only two decay modes, i.e., $\nu_H \to \nu_e e^+ e^-$ and $\nu_H \to \sum_{\beta=e,\mu,\tau} \nu_e \bar{\nu}_\beta \nu_\beta$. The ratio of the decay rates for the two modes is defined with Eqs. (A15) and (A27) as

$$R_\text{dec} = \frac{\Gamma(\nu_H \to \nu_e e^+ e^-)}{\Gamma(\nu_H \to \sum_\beta \nu_e \bar{\nu}_\beta \nu_\beta)}. \quad (4.8)$$

Through the two decay modes, energetic neutrinos, electrons, and positrons are generated. The ratio of average total energies of ν and $e^\pm$ emitted through the two decay modes is given by

$$R(\nu, e) = \frac{1 + R_\text{dec} f_E(\nu_e)}{R_\text{dec}[f_E(e^-) + f_E(e^+)]}, \quad (4.9)$$

where $f_E(i) = \bar{E}_i / M_{\nu_H}$ is the ratio of the average energy of species i to the sterile neutrino mass in the decay mode of $\nu_H \to \nu_e e^+ e^-$, and the equation, $f_E(\nu_e) + f_E(e^-) + f_E(e^+) = 1$ is satisfied. There is a trivial relation between parameters:
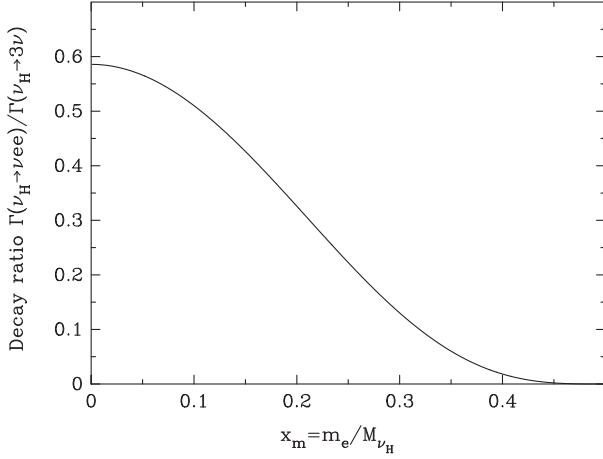
FIG. 2. The ratio of the decay rates $R_{\mathrm{dec}} = \Gamma(\nu_{\mathrm{H}} \to \nu_e e^+ e^-)/\Gamma(\nu_{\mathrm{H}} \to \sum_\beta \nu_e \bar{\nu}_\beta \nu_\beta)$ as a function of $x_{\mathrm{m}} = m_e/M_{\nu_{\mathrm{H}}}$.

$$\frac{\zeta_{\nu_{\mathrm{H}} \to \nu}}{\zeta_{\nu_{\mathrm{H}} \to e}} = R(\nu, e), \tag{4.10}$$

where $\zeta_{\nu_{\mathrm{H}} \to \nu} = (n_{\nu_{\mathrm{H}}}^0/n_\gamma^0) E_{\nu_{\mathrm{H}} \to \nu}$ is defined.

Figure 2 shows the ratio of the decay rates R_{dec} as a function of $x_{\mathrm{m}} = m_e/M_{\nu_{\mathrm{H}}}$. When the sterile neutrino mass is much larger than the electron mass, i.e., $x_{\mathrm{m}} \ll 0.5$, the rate for the decay into $\nu_e e^+ e^-$ is comparable to that into three neutrinos. The ratio monotonically decreases with increasing x_{m}. When the sterile neutrino mass is nearly one half of the electron mass, i.e., $x_{\mathrm{m}} \approx 0.5$, this ratio becomes very small and the decay into three neutrinos dominates.

Figure 3 shows the ratio of average total energies of neutrinos and $e^\pm$'s injected at the sterile neutrino decay $R(\nu, e)$ as a function of x_{m}. In the large limit of the sterile neutrino mass, $x_{\mathrm{m}} \ll 1$, the ratio approaches to $\sim 10^{0.5} = 3.16$. The ratio monotonically increases with increasing x_{m}. The ratio diverges in the small mass limit, $x_{\mathrm{m}} \to 0.5$.

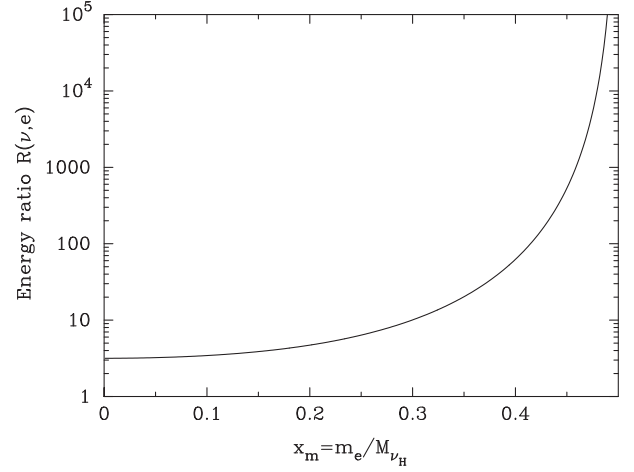Equation of the energy conservation is given [Eq. (D.26) of Ref. [58]] by

FIG. 3. The ratio of average total energies of neutrinos and $e^\pm$'s injected at the sterile neutrino decay $R(\nu, e)$ [Eq. (4.9)] as a function of $x_{\mathrm{m}} = m_e/M_{\nu_{\mathrm{H}}}$.

$$\frac{d}{dt}(\rho a^3) + p \frac{d}{dt}(a^3) + a^3 \frac{d\rho}{dt}\bigg|_{T_9}^{\mathrm{nuc}} + \frac{d(a^3 \rho_{\nu_{\mathrm{H}}})}{dt}\bigg|_{T_9}^{\mathrm{dec}} = 0, \tag{4.11}$$

where p is the total pressure of the Universe, and the third and fourth terms in the left-hand side correspond to the energy changes by nucleosynthesis and the electromagnetic energy injection at the sterile neutrino decay, respectively. The term of the electromagnetic energy injection is given by

$$\frac{d(a^3 \rho_{\nu_{\mathrm{H}}})}{dt}\bigg|_{T_9}^{\mathrm{dec}} = -\frac{a^3 \rho_{\nu_{\mathrm{H}}}}{\tau_{\nu_{\mathrm{H}}}} \frac{E_{\nu_{\mathrm{H}} \to e}}{M_{\nu_{\mathrm{H}}}}. \tag{4.12}$$

The equation of the energy conservation is then transformed to

$$\frac{dr}{dT_9} = -\frac{\frac{d\rho_\gamma}{dT_9} + \frac{d\rho_e}{dT_9} + \frac{d\rho_b}{dT_9}}{\rho_\gamma + p_\gamma + \rho_e + p_e + p_b + \frac{1}{dr/dt}\left(\frac{d\rho_b}{dt}\big|_{T_9}^{\mathrm{nuc}} + \frac{d\rho_e}{dt}\big|_{T_9}^{\mathrm{nuc}} - \frac{\rho_{\nu_{\mathrm{H}}}}{\tau_{\nu_{\mathrm{H}}}} \frac{E_{\nu_{\mathrm{H}} \to e}}{M_{\nu_{\mathrm{H}}}}\right)}, \tag{4.13}$$

where $r = \ln(a^3)$ is defined; $dr/dt = 3H$; and $\rho_e = \rho_{e^-} + \rho_{e^+}$ and $p_e = p_{e^-} + p_{e^+}$ are the total energy density and pressure, respectively, of electrons and positrons. This is a varied form of the temperature evolution as a function of time, dT_9/dt [cf. Eq. (22) of Ref. [93][, and is used in Kawano's BBN code. The last term in the brackets in the denominator of the rhs is absent unless the entropy production is induced by the ν_{H} decay [cf. Eq. (D.28) of Ref. [58]].

B. Effective neutrino number

The effective neutrino number is defined by

$$N_{\mathrm{eff}} = \frac{\rho_\nu}{\frac{7\pi^2}{120}\left(\frac{4}{11}\right)^{4/3} T^4}, \tag{4.14}$$

where $\rho_\nu = \rho_{\nu,\mathrm{th}} + \rho_{\nu,\mathrm{nt}}$ is the total neutrino energy density.

The thermal neutrinos interact with thermal bath until the temperature decreases to $T \sim 1$ MeV. Then, they decouple

from background photons at $T \sim 1$ MeV and have temperature T_ν, which can be different from the photon temperature T. The energy density of the thermal neutrinos is given by

$$\rho_{\nu,\text{th}} = \frac{7\pi^2}{120} N_{\text{eff,i}} T_\nu^4, \tag{4.15}$$

where $N_{\text{eff,i}} = 3$ is the effective neutrino number at the initial time $M_{\nu_\text{H}} \gg t_\text{i} > \mathcal{O}(1)$ MeV before the cosmological $e^\pm$ annihilation.

The nonthermal neutrinos are assumed to originate only from the ν_H decay. Since we assume that the decay occurs much later than the BBN epoch, nonthermal neutrinos from the decay cannot be thermalized typically. The nonthermal neutrinos, therefore, need to be treated separately from the thermal ones. The photon number density is given by

$$n_\gamma = \frac{2\zeta(3)}{\pi^2} T(t)^3. \tag{4.16}$$

Using Eqs. (4.6), (4.14), (4.15), and (4.16), the effective neutrino number is transformed to

$$N_{\text{eff}} = \left(\frac{11}{4}\right)^{4/3} \left(\frac{T_\nu}{T}\right)^4 N_{\text{eff,i}} + \frac{240\zeta(3)}{7\pi^4} \left(\frac{11}{4}\right)^{7/3}$$
$$\times \frac{\zeta_{\nu_\text{H}\to\nu}}{\tau_{\nu_\text{H}}} \frac{T(t_\text{i})^3}{T^4} \frac{a_\text{i}^3}{a(t)^4} \int_{t_\text{i}}^t a(t') e^{-t'/\tau_{\nu_\text{H}}} dt'. \tag{4.17}$$

We use $T(t_\text{i}) = T_\nu(t_\text{i})$ and $a(t) T_\nu(t) = \text{constant}$. The effective neutrino number can then be described as

$$N_{\text{eff}} = \left(\frac{11}{4}\right)^{4/3} \left(\frac{T_\nu}{T}\right)^4 \left[N_{\text{eff,i}} + \frac{240\zeta(3)}{7\pi^4} \left(\frac{11}{4}\right)\right.$$
$$\left. \times \int_{t_\text{i}}^t \frac{\zeta_{\nu_\text{H}\to\nu}}{T_\nu(t')} e^{-t'/\tau_{\nu_\text{H}}} \frac{dt'}{\tau_{\nu_\text{H}}}\right]. \tag{4.18}$$

The factor $(11/4)^{4/3}(T_\nu/T)^4$ in the rhs results from the entropy production by the injection of nonthermal electrons and positrons at the ν_H decay. The number and energy densities of thermal neutrinos for a fixed photon temperature T are decreased compared to the case of no entropy production. The second term in the square brackets corresponds to an increase of the neutrino energy density contributed by the nonthermal active neutrino injection.

The time derivative of the effective neutrino number can be derived from this equation as

$$\frac{dN_{\text{eff}}}{dt} = 4N_{\text{eff}} \left(\frac{d\ln T_\nu}{dt} - \frac{d\ln T}{dt}\right)$$
$$+ \left(\frac{11}{4}\right)^{7/3} \left(\frac{T_\nu}{T}\right)^4 \frac{240\zeta(3)}{7\pi^4} \frac{\zeta_{\nu_\text{H}\to\nu}}{T_\nu} e^{-t/\tau_{\nu_\text{H}}} \frac{1}{\tau_{\nu_\text{H}}}. \tag{4.19}$$

Then, we solve the time evolution of the effective neutrino number simultaneously with those of $a(t)$ [Eq. (4.5)], $T(t)$ [Eq. (4.13)], and $T_\nu(t) \propto a(t)^{-1}$.

C. Baryon-to-photon ratio

An injection of energetic $e^\pm$ at the ν_H decay produces nonthermal photons via electromagnetic cascade showers, and enhances the comoving photon entropy in the Universe. Since the baryon-to-photon ratio η is inversely proportional to the comoving photon entropy, the ratio is reduced as a function of time during the nonthermal photon injection [95,98]. In this case, the η value in the BBN epoch is larger than that in the epoch of the CBR last scattering. We adopt the baryon-to-photon ratio inferred from Planck measurement of CBR as the value after the ν_H decay. The initial η value is then determined as a function of τ_{ν_H} and $\zeta_{\nu_\text{H}\to e}$ such that it results in the final η value consistent with the Planck data. Here we define the following variables: The time t_bef is between the cosmological $e^\pm$ annihilation epoch and the ν_H decay, while the time t_aft is after the decay. The quantities $S_{\gamma,\text{bef}}$ and $S_{\gamma,\text{aft}}$ are the comoving photon entropies at times t_bef and t_aft, respectively, while η_bef and η_aft are baryon-to-photon ratios at times t_bef and t_aft, respectively.

The comoving entropy density is given [99] by

$$S = g_{*\text{S}} a^3 T^3, \tag{4.20}$$

where $g_{*\text{S}}$ is the relativistic d.o.f. in terms of entropy. Since we consider the ν_H decay after the neutrino decoupling at $T \sim 1$ MeV, the photon is the only relativistic component in the thermal bath. Therefore, this d.o.f. is the same as the statistical d.o.f. of the photon, i.e., $g_{*\text{S}} = g_\gamma = 2$. The scale factor of the Universe is inversely proportional to the neutrino temperature. The ratio of the comoving photon entropies $S_\gamma/S_{\gamma,\text{bef}} = \eta_\text{bef}/\eta$ is, therefore, given by

$$\frac{S_\gamma}{S_{\gamma,\text{bef}}} = \left(\frac{T_{\nu,\text{bef}}}{T_\text{bef}}\right)^3 \left(\frac{T}{T_\nu}\right)^3$$
$$= \left(\frac{4}{11}\right) \left(\frac{T}{T_\nu}\right)^3, \tag{4.21}$$

where $T_{\nu,\text{bef}}$ is the neutrino temperature before the ν_H decay, and we used the relation $T_{\nu,\text{bef}}/T_\text{bef} = (4/11)^{1/3}$.

The Planck measurement has obtained the $\Omega_b h^2$ value from the combined data of Planck + WP + highL + BAO: $\Omega_b h^2 = 0.02214 \pm 0.00024$ (68% C.L.) [8]. Therefore, the error in the baryon-to-photon ratio [Eq. (2.4)] or the comoving entropy at the CBR last scattering is lower than 2.2% (2σ).

D. Approximate formulas

1. Baryon-to-photon ratio

When the comoving photon entropy changes by a small fraction, i.e., $\ll 100\%$ in the epoch of the ν_H decay, the

ratio $S_{\gamma,\mathrm{aft}}/S_{\gamma,\mathrm{bef}} = \eta_{\mathrm{bef}}/\eta_{\mathrm{aft}}$ is approximately given [98] by

$$\frac{S_{\gamma,\mathrm{aft}}}{S_{\gamma,\mathrm{bef}}} = \exp\left[\frac{45^{3/4}\zeta(3)}{\pi^{11/4}}\frac{(g_*^{\tau_{\nu_\mathrm{H}}})^{1/4}}{g_{\gamma*S}^{\mathrm{bef}}}\frac{E_{\nu_\mathrm{H}\to e}n_{\nu_\mathrm{H}}^{\mathrm{bef}}}{n_\gamma^{\mathrm{bef}}}\sqrt{\frac{\tau_{\nu_\mathrm{H}}}{M_{\mathrm{Pl}}}}\right], \tag{4.22}$$

where $g_*^{\tau_{\nu_\mathrm{H}}} = 3.36$ and $g_{\gamma*S}^{\mathrm{bef}} = g_\gamma = 2$ are the relativistic d.o.f.'s in terms of energy and entropy, respectively, after the BBN epoch; $n_{\nu_\mathrm{H}}^{\mathrm{bef}}$ and n_γ^{bef} are number densities of the decaying particle and photon, respectively, evaluated at the same time t_{bef}; and $M_{\mathrm{Pl}} = G_{\mathrm{N}}^{-1/2} = 1.22 \times 10^{19}$ GeV is the Planck mass. The $g_{\gamma*S}^{\mathrm{bef}}$ value is the same as the statistical d.o.f. of the photon [100]. For a small fractional change of entropy, this value is given [98] by

$$\frac{\Delta S_\gamma}{S_\gamma} \approx \ln\frac{S_{\gamma,\mathrm{aft}}}{S_{\gamma,\mathrm{bef}}} = 2.14 \times 10^{-4}\left(\frac{\zeta_{\nu_\mathrm{H}\to e}}{10^{-9}\ \mathrm{GeV}}\right)\left(\frac{\tau_{\nu_\mathrm{H}}}{10^6\ \mathrm{s}}\right)^{1/2}. \tag{4.23}$$

The ratio of the baryon-to-photon ratios $\eta_{\mathrm{aft}}/\eta_{\mathrm{bef}} = S_{\gamma,\mathrm{bef}}/S_{\gamma,\mathrm{aft}}$ can be estimated using this formula.

2. Neutrino number

The energy density of nonthermal active neutrinos is generated by the ν_H decay, and an approximate formula can be derived as in the case of a nonthermal photon injection in the late Universe [101]. It is assumed that the sterile neutrino does not contribute to the total energy density so much that the cosmic expansion rate is not affected much. The standard radiation dominated Universe then holds. We define the second term in the square brackets of Eq. (4.18) as $N_{\mathrm{eff,nt,i}}$. This term then approximately becomes

$$N_{\mathrm{eff,nt,i}} = \frac{240\zeta(3)}{7\pi^4}\left(\frac{11}{4}\right)\frac{\zeta_{\nu_\mathrm{H}\to\nu}}{T_\nu(t_{\mathrm{eff}})}$$
$$\approx \frac{240\zeta(3)}{7\pi^4}\left(\frac{11}{4}\right)^{4/3}\frac{\zeta_{\nu_\mathrm{H}\to\nu}}{T(t_{\mathrm{eff}})}, \tag{4.24}$$

where the effective time is defined as $t_{\mathrm{eff}} = [\Gamma(1+\beta)]^{1/\beta}\tau_{\nu_\mathrm{H}}$ for the Universe with the time-temperature relation of $T \propto t^{-\beta}$ with $\Gamma(x)$ the gamma function of argument x [102]. For the radiation dominated Universe considered here, $\beta = 1/2$ and $t_{\mathrm{eff}} = (\pi/4)\tau_{\nu_\mathrm{H}}$ are satisfied.

If the nonthermal neutrino injection is not accompanied by the nonthermal photon injection, the photon heating never occurs and the effective neutrino number after the decay is $N_{\mathrm{eff}} = N_{\mathrm{eff,i}} + N_{\mathrm{eff,nt,i}}$. On the other hand, when nonthermal electrons and positrons are injected at the ν_H decay, the entropy of the Universe is increased. The number and energy densities of neutrinos for a fixed photon temperature T are then decreased compared to the case of no entropy production. The effective number after the decay is given [94] by

$$N_{\mathrm{eff}} = \left(\frac{11}{4}\right)^{4/3}\left(\frac{T_\nu}{T}\right)^4(N_{\mathrm{eff,i}} + N_{\mathrm{eff,nt,i}})$$
$$= \left(\frac{S_{\gamma,\mathrm{aft}}}{S_{\gamma,\mathrm{bef}}}\right)^{-4/3}(N_{\mathrm{eff,i}} + N_{\mathrm{eff,nt,i}}). \tag{4.25}$$

An approximate solution of N_{eff} is then derived with Eqs. (4.23), (4.24), and (4.25).

V. OBSERVATIONAL CONSTRAINTS

We constrain the model of the decaying sterile neutrino by comparing calculated results and observational constraints on elemental abundances, the effective neutrino number, and the CMB energy spectrum.

A. Light element abundances

In this model, $^7\mathrm{Be}$ is disintegrated by nonthermal photons originating from the ν_H decay. Since a primordial abundance of $^7\mathrm{Li}$ is mainly contributed from that of $^7\mathrm{Be}$ produced during the BBN epoch, the destruction of $^7\mathrm{Be}$ reduces the final $^7\mathrm{Li}$ abundance. However, the energies of nonthermal photons should be small since energetic photons can disintegrate other nuclei and result in an inconsistency with observed abundances. In the case of low energy photons, abundances of only D, $^7\mathrm{Li}$, and $^7\mathrm{Be}$ can be significantly affected because of their small threshold energies for photodisintegration [35]. If the photon energy is larger (4 MeV$< E_\gamma < 20$ MeV), the photodisintegration of $^6\mathrm{Li}$, $^3\mathrm{He}$, and $^3\mathrm{H}$, and the production of $^6\mathrm{Li}$ via $^7\mathrm{Be}(\gamma, p)^6\mathrm{Li}$ and $^7\mathrm{Li}(\gamma, n)^6\mathrm{Li}$ are also possible. In addition, the time evolution of the baryon-to-photon ratio induced by the ν_H decay changes light element abundances from the values in SBBN. Therefore, we adopt the following constraints for respective light nuclides. It is noted that only the constraints on D and $^7\mathrm{Li}$ abundances are important while other constraints are not in deriving constraints in the parameter plane of this model with the decaying sterile neutrino of $M_{\nu_\mathrm{H}} \sim 10$–20 MeV (Sec. VI B).

We use the primordial D abundance determined from observations of quasistellar object (QSO) absorption systems. As conservative constraints, the 2σ and 4σ ranges estimated with the mean value of ten Lyman-α absorption systems, $\log(\mathrm{D/H}) = -4.58 \pm 0.02\ (1\sigma)$ [103], are adopted.

$^3\mathrm{He}$ abundances are measured in Galactic H II regions through the $^3\mathrm{He}^+$ 8.665 GHz hyperfine transition line, $^3\mathrm{He/H} = (1.9 \pm 0.6) \times 10^{-5}\ (1\sigma)$ [104]. Since this is an abundance at high metallicity, and Galactic chemical evolution of $^3\mathrm{He}$ is largely uncertain, this abundance is not used as a constraint on the primordial abundance in this study. In this model, however, the $^3\mathrm{He}$ abundance is never changed significantly. Therefore, the $^3\mathrm{He}$ abundance cannot be constrained from observations anyway.

Primordial $^4\mathrm{He}$ abundance has been derived by two different observations of metal-poor extragalactic H II regions: $Y_\mathrm{p} = 0.2565 \pm 0.0051\ (1\sigma)$ [105] and

$Y_p = 0.2561 \pm 0.0108$ (1σ) [106]. We take 2σ limits from the latter conservative result with a large error bar.

Primordial ^{7}Li abundance is taken from a determination by spectroscopic observations of MPSs. The observed abundances are about three times smaller than theoretical values in the SBBN model. We adopt the observational limit, $\log(^7\text{Li/H}) = -12 + (2.199 \pm 0.086)$ (1σ) derived in a 3D nonlocal thermal equilibrium model [18]. We should consider the possibility that ^{7}Li abundances in surfaces of MPSs are depleted by a factor of $\lesssim 2$ as suggested by calculations of a stellar model with a turbulent mixing [32–34]. Below we find that the ^{7}Li abundance in this model cannot be consistent with the observational 2σ limit. When the ^{7}Li depletion occurs in the stellar surfaces, however, some degree of ^{7}Li reduction in this model can explain the observation.

^{6}Li abundances are measured in observations of MPSs. A recent analysis, however, does not indicate any detection of this isotope [107]. Since ^{6}Li nuclei can be reasonably produced and destroyed after BBN, its primordial abundance is chosen conservatively. We use the least stringent 2σ upper limit among those for all stars reported in Ref. [107]: $^6\text{Li/H} = (0.9 \pm 4.3) \times 10^{-12}$ (1σ) for the G64-12 (nonlocal thermal equilibrium model with five free parameters).

B. Effective neutrino number

The effective neutrino number has been constrained from CMB observations. We adopt the latest limit derived from the combined data of Planck + WP + highL + BAO for the one-parameter extension to the base ΛCDM model: $N_{\text{eff}} = 3.30^{+0.54}_{-0.51}$ (95% C.L.) [8]. This one-parameter extension model is different from the present model of the decaying sterile neutrino in terms of cosmic expansion rates and the time evolutions of N_{eff} values. In the former model, relativistic particles are added to the standard ΛCDM model, while in the latter, the nonrelativistic ν_H and its decay are assumed. The above limit, therefore, cannot be applied to the present model as it is. This limit, however, mainly comes from effects of the radiation energy density around the matter-radiation equal time. Since the equal time is much later than the decay lifetime of the sterile neutrino $\tau_{\nu_H} \lesssim 10^6$ s (see Sec. III) considered in this paper, the above limit approximately gives a limit on the final N_{eff} value in this decaying ν_H model.

C. CMB energy spectrum

An injection of nonthermal photons to the thermal bath triggers a deformation of the CBR spectrum from the blackbody spectrum [101]. Such a deformation is severely constrained by observations which indicate a nearly complete Planck spectrum [108]. We adopt the most stringent limits on the chemical potential and the Compton y parameter from the analysis of the data from the Far-Infrared Absolute Spectrophotometer on board the Cosmic

Background Explorer, $|\mu| < 9 \times 10^{-5}$ and $|y| < 1.5 \times 10^{-5}$, respectively [108].

VI. RESULTS

A. Nonthermal photon spectra

Figure 4 shows normalized energy spectra of electrons [Eq. (A10)] and positrons [Eq. (A11)] generated at the ν_H decay, and the total spectrum (multiplied by $1/2$) as a function of $x_e = 2E_e/M_{\nu_H}$, with E_e the energies of electron and positron. For all figures in this subsection, we assume that the mass of the sterile neutrino is $M_{\nu_H} = 14$ MeV since we find that this mass is included in the most important mass region for ^{7}Be photodisintegration in the present model (see Sec. VI B). Functions $f_1(x_e)$, $f_2(x_e)$, and $f_3(x_e)$ [cf. Eqs. (A12)–(A14)] are also shown. Because of these extended energy spectra of $e^\pm$'s, nonthermal photons produced via inverse Compton scattering of CBR by the generated $e^\pm$'s also have extended energy spectra.

Figure 5 shows energy spectra of the primary photon produced via the inverse Compton scattering of electrons and positrons which are generated at the decay for the cosmic photon temperature of $T = 1$, 10, and 100 keV, respectively. The primary photon spectra are given by

$$p_\gamma^{\text{pri}}(E_{\gamma 0}; T, M_{\nu_H}) = \frac{1}{\Gamma} \int_{m_e}^{M_{\nu_H}/2} \frac{d\Gamma}{dE_e}(M_{\nu_H}) P_{\text{iC}}(E_e, E_{\gamma 0}; T) dE_e.$$

(6.1)

When the energy injection with given spectra (Fig. 4) occurs at lower temperatures, the inverse Compton scattering produces softer spectra of nonthermal primary photon, and cutoff energies are lower [cf. Eq. (2.14); positions of
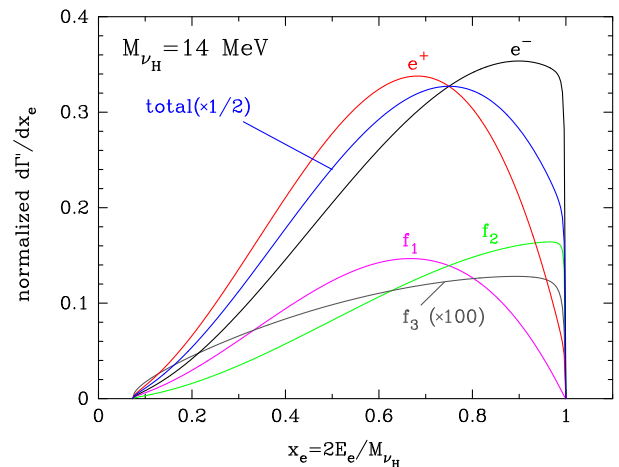

FIG. 4 (color online). Normalized energy spectra of electrons [Eq. (A10)] and positrons [Eq. (A11)] generated at the ν_H decay, and the total spectrum. Functions $f_1(x_e)$, $f_2(x_e)$, and $f_3(x_e)$ [cf. Eqs. (A12)–(A14)] are also shown. The mass of the sterile neutrino is assumed to be $M_{\nu_H} = 14$ MeV.
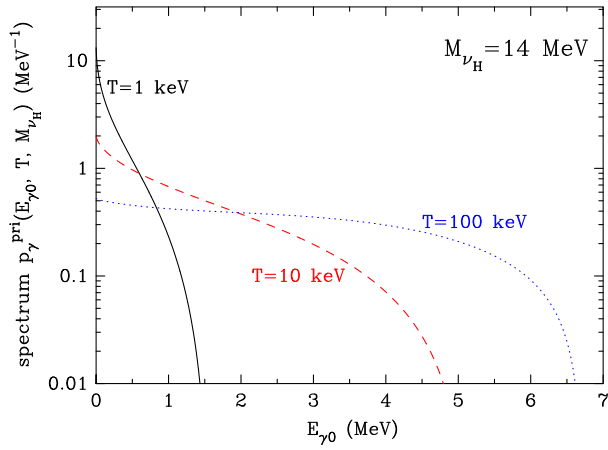
FIG. 5 (color online). Energy spectra of the primary photon produced via the inverse Compton scattering of electrons and positrons which are generated at the decay for the cosmic photon temperature of $T = 1$, 10, and 100 keV, respectively. The mass of the sterile neutrino is assumed to be $M_{\nu_H} = 14$ MeV.

cutoff are not seen in this figure]. These results reflect the differential inverse Compton scattering rate [Eq. (2.16)].

Figure 6 shows injection spectra of nonthermal photons formed through the electromagnetic cascade calculated with Eq. (2.8) for $T = 1$, 3, and 10 keV, respectively. As the temperature decreases, the primary photon spectrum $p_\gamma^{\rm pri}$ becomes softer so that fewer photons have high enough energies to disintegrate ^{7}Be. The spectrum of photons secondarily induced by the primary photons, however, has an upper cutoff at $E_C \sim m_e^2/(22T)$ [41], which scales as an inverse of the temperature. Therefore, the cutoff energy is larger at lower temperature. The cutoff can be seen at $E_\gamma \sim 1.15$ MeV for $T = 10$ keV. Because of the combination of the softness of the primary photon spectrum and the cutoff energy in an electromagnetic cascade shower, there is a best
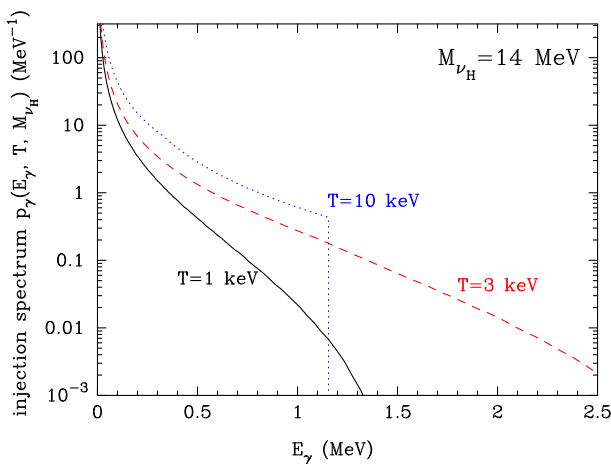
temperature of the energy injection where relatively large abundances of energetic photons are produced with $E_\gamma > 1.59$ MeV, which can destroy ^{7}Be. One can find that the best temperature is 3 keV among the three temperatures shown in this figure.

B. Light element abundances, $N_{\rm eff}$, and CMB energy spectrum

Figure 7 shows contours for calculated abundances of D and ^{7}Li in the $(\tau_{\nu_H}, \zeta_{\nu_H \to e})$ plane for $M_{\nu_H} = 14$ MeV. The two curved diagonal solid lines marked as "D low (2σ)" and "(4σ)" correspond to the observational 2σ and 4σ limits, respectively, on the D abundance. The regions above the lines are excluded by D underproduction. Solid sharp curves at $\tau_{\nu_H} \sim 10^5$ s are contours for the reduction ratio of ^{7}Li abundance defined as

$$\Delta^7{\rm Li} = \frac{(^7{\rm Li/H}) - (^7{\rm Li/H})_{\rm SBBN}}{(^7{\rm Li/H})_{\rm SBBN}}, \qquad (6.2)$$

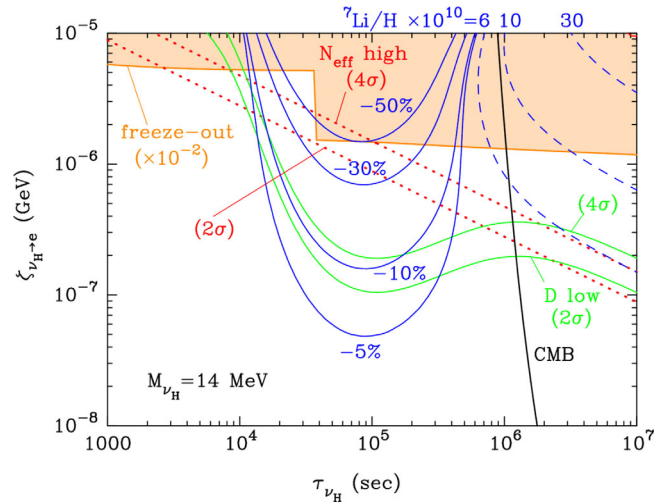where $(^7{\rm Li/H})$ is the abundance calculated in this model, and $(^7{\rm Li/H})_{\rm SBBN} = 5.07 \times 10^{-10}$ is the SBBN value.

FIG. 7 (color online). Contours for calculated abundances of D and ^{7}Li in the parameter plane of $(\tau_{\nu_H}, \zeta_{\nu_H \to e})$ for $M_{\nu_H} = 14$ MeV. The regions above the curved diagonal solid lines marked as "D low (2σ)" and "(4σ)" are excluded by D underproduction compared to the observational constraints at 2σ and 4σ levels, respectively. The calculated ^{7}Li abundance is smaller than the SBBN value above solid sharp curves at $\tau_{\nu_H} \sim 10^5$ s by percentages shown near the curves, while it is larger above the dashed curves. The dotted lines show the 2σ and 4σ upper limits on the effective neutrino number at the cosmological recombination epoch from the CMB power spectrum. The right region from the nearly vertical solid line labeled as "CMB" is excluded from the limits from the CMB energy spectrum. The shaded region corresponds to thermal freeze-out ν_H abundances with a possible ν_H dilution by a factor of 100 taken into account (see Secs. VII A and VII B).

FIG. 6 (color online). Injection spectra of the nonthermal photon formed through the electromagnetic cascade for $T = 1$, 3, and 10 keV, respectively. The mass of the sterile neutrino is assumed to be $M_{\nu_H} = 14$ MeV.
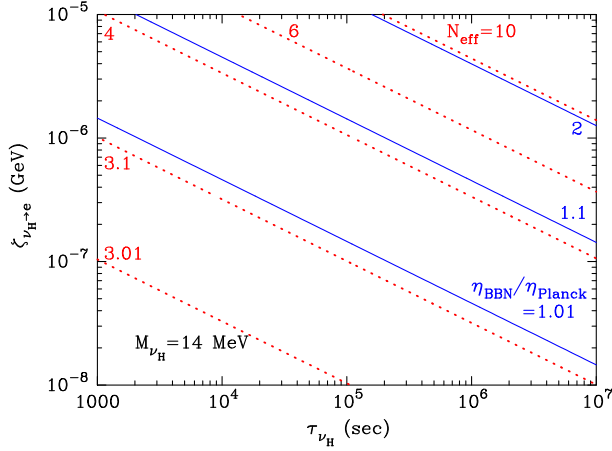
FIG. 8 (color online).   Contours of the ratio between the baryon-to-photon ratios in the BBN epoch and the cosmological recombination epoch (solid lines), and contours of the $N_{\rm eff}$ value in the cosmological recombination epoch after the sterile neutrino decay in the parameter plane of $(\tau_{\nu_{\rm H}}, \zeta_{\nu_{\rm H}\to e})$ for $M_{\nu_{\rm H}} = 14$ MeV.

FIG. 9 (color online).   Same as in Fig. 7 but for $M_{\nu_{\rm H}} = 12$ MeV.

Dashed curves are, on the other hand, contours for the calculated abundances (^{7}Li/H). Inside the solid curves for ^{7}Li, the calculated ^{7}Li abundance is smaller than the SBBN value because of the ^{7}Be photodisintegration. The ^{7}Li abundance is larger above the dashed curves than the SBBN value because of the larger η value during the BBN epoch.

The dotted lines show the 2σ and 4σ upper limits on the effective neutrino number at the cosmological recombination epoch from the CMB power spectrum. The nearly vertical solid line labeled as "CMB" corresponds to the limits on the CMB energy spectrum. The right region from this line (long lifetime $\tau_{\nu_{\rm H}} \gtrsim 10^6$ s) is excluded from a large deformation in the energy spectrum. We note that in the parameter region shown in Fig. 7, this model is constrained exclusively from the limit on the CMB μ parameter.

Figure 8 shows contours of the ratio between the baryon-to-photon ratios in the BBN epoch and the cosmological recombination epoch (solid lines), and contours of the $N_{\rm eff}$ value in the cosmological recombination epoch after the sterile neutrino decay in the parameter plane of $(\tau_{\nu_{\rm H}}, \zeta_{\nu_{\rm H}\to e})$ for $M_{\nu_{\rm H}} = 14$ MeV.

The parameter region for small ^{7}Li abundance is found at $\tau_{\nu_{\rm H}} \sim 10^4$–$10^5$ s and $\zeta_{\nu_{\rm H}\to e} \sim 10^{-6}$–$10^{-7}$ GeV. In the epoch between the BBN and the matter radiation equality, the photon temperature in the Universe T is related to the cosmic age t as $T = 1.15$ keV $(t/10^6$ s$)^{-1/2}$ unless the cosmic expansion rate is significantly affected by the sterile neutrino. If the $\nu_{\rm H}$ decay occurs at $T = \mathcal{O}(1$ keV$)$, the ^{7}Li abundance is reduced most effectively although some amount of D destruction always occurs simultaneously. The shapes of contours of D and ^{7}Li are explained as follows. At short lifetimes of $\tau_{\nu_{\rm H}} \lesssim 10^4$ s, the upper cutoff of the nonthermal photon spectrum $E_C \sim m_e^2/(22T)$ [41] is
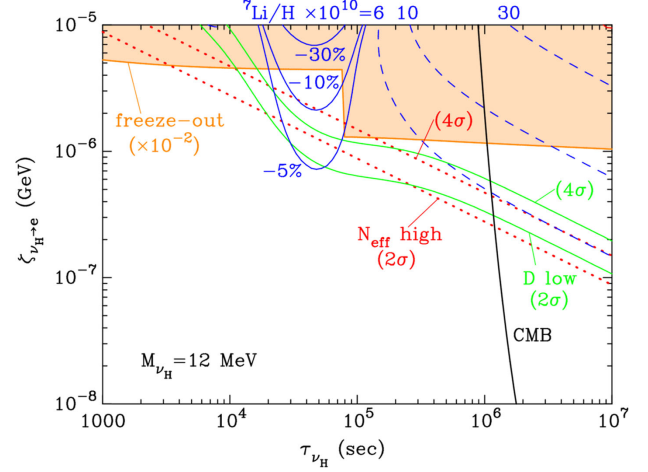
smaller than threshold energies for photodisintegration of light nuclides $E_{\gamma,{\rm th}} \sim \mathcal{O}(1-10)$ MeV. Effects of nonthermal photons on elemental abundances are, therefore, negligibly small. At longer lifetimes of $\tau_{\nu_{\rm H}} \gtrsim 10^5$ s, on the other hand, primary photons produced via the inverse Compton scattering have softer energy spectra and lower cutoff energy originating from the maximum energy of the scattered photon [Eq. (2.14)]. This fact results in smaller abundances of nonthermal photons which are energetic enough to destroy D and ^{7}Li. As a result, effects of nuclear photodisintegration are less efficient in the long lifetime region also.

The lower solid line of D is located between the solid curves of $\Delta^7{\rm Li} = -5\%$ and -10% in the interesting parameter region. It means that in this region, the ^{7}Be photodisintegration can slightly reduce the primordial ^{7}Li abundance down to nearly the observational 2σ upper limit multiplied by the stellar depletion factor of 2. The D abundance, however, simultaneously decreases down to the observational 2σ lower limit. We then find that there is no parameter region in which primordial ^{7}Li abundance can be consistent with the MPS value without assuming a stellar depletion. This model, however, provides a mechanism of ^{7}Li reduction by some small factor with its signatures imprinted in the primordial D abundance and the effective neutrino number (Sec. VI D).

Figures 9 and 10 show contours for calculated abundances of D and ^{7}Li, the effective neutrino number, and the CMB μ parameter as in Fig. 7, but for $M_{\nu_{\rm H}} = 12$ and 17 MeV, respectively. As seen in Figs. 7, 9, and 10, regions of D and ^{7}Li destruction at $\tau_{\nu_{\rm H}} \sim 10^5$ s are located at lower positions for larger masses. This is because the sterile neutrinos with smaller masses can generate smaller numbers of energetic $e^\pm$'s which trigger D and ^{7}Li destruction. Since the energy fraction of energetic photons capable of destroying ^{7}Be to total nonthermal photons is smaller, we need a larger total energy generated at the $\nu_{\rm H}$ decay. Such a large energy injection is, however, constrained from BBN
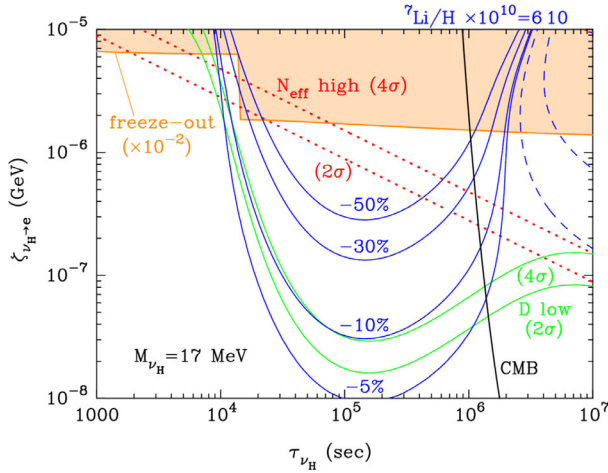
FIG. 10 (color online). Same as in Fig. 7 but for $M_{\nu_H} = 17$ MeV.

FIG. 11 (color online). Transfer functions $G^1_{[P\gamma]_A}(T; 14 \text{ MeV})$ [Eq. (2.29)] calculated with the new (thick lines) and old (thin lines) cross sections of $^7\text{Be}(\gamma,\alpha)^3\text{He}$ and $^7\text{Li}(\gamma,\alpha)^3\text{H}$ as a function of T_9.

results taking into account the change of the baryon-to-photon ratio from the CMB-inferred value (Sec. IV C). Therefore, for $M_{\nu_H} < 14$ MeV the photodisintegration is less effective than the change of the baryon-to-photon ratio, and no parameter region for ^7Li reduction is found. The mass of $M_{\nu_H} \gtrsim 14$ MeV is thus the best case for ^7Be reduction that is a partial solution to the Li problem.

The parameter region for the small primordial ^7Li abundance is about to be excluded from observational constraint on D abundance. In this parameter region, the change of D abundance partially originates from the change of the baryon-to-photon ratio. In the case of smaller M_{ν_H} values, the change of the baryon-to-photon ratio is more significant. In the interesting parameter region, the effective neutrino number is also affected. Therefore, this model for the ^7Li reduction will be tested through observational determinations of the effective neutrino number (Sec. IV B) in the near future.

C. Impact of revised cross sections

We compare results of nonthermal nucleosynthesis calculated with the new and old cross sections of $^7\text{Be}(\gamma,\alpha)^3\text{He}$ and $^7\text{Li}(\gamma,\alpha)^3\text{H}$. Old cross sections have been adopted from the fitted functions in Ref. [44]. For the reaction $^7\text{Be}(\gamma,\alpha)^3\text{He}$, the cross section is set to be zero for 5.41 MeV $< E_\gamma$ since the function gives negative values.

Figure 11 shows the transfer functions $G^1_{[P\gamma]_A}(T; 14 \text{ MeV})$ [Eq. (2.29)] calculated with the new (thick lines) and old (thin lines) cross sections as a function of T_9. The new transfer function of $^7\text{Be}(\gamma,\alpha)^3\text{He}$ is 2.3 times smaller than the old one, while that of $^7\text{Li}(\gamma,\alpha)^3\text{H}$ is 2.5 times smaller than the old one at their peak positions. These changes are caused mainly by the fact that the new cross sections at low energies near the photodisintegration threshold energies are about one third of the old ones (Fig. 1).
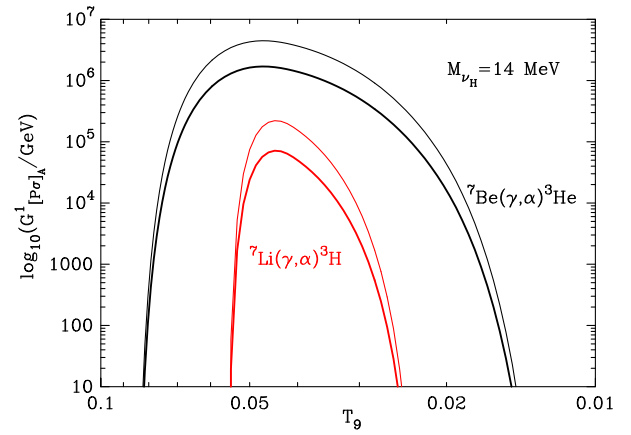
Figure 12 shows the same contours for calculated abundances of D and ^7Li, the effective neutrino number, and the CMB μ parameter as in Fig. 7 for $M_{\nu_H} = 14$ MeV, but for results calculated with old cross sections. Solid lines for ^7Li are located in the lower positions than those in Fig. 7. This is because the adopted cross sections of $^7\text{Be}(\gamma,\alpha)^3\text{He}$ and $^7\text{Li}(\gamma,\alpha)^3\text{H}$ are smaller, and as a result, the photodisintegration rates are smaller (Fig. 11). We note that when old cross sections are used carelessly, one finds a fake parameter region in which ^7Li abundance can be significantly reduced without a large efficiency of D photodisintegration, as shown in this figure. It is, therefore, necessary to adopt the precise cross sections of the reactions $^7\text{Be}(\gamma,\alpha)^3\text{He}$ and $^7\text{Li}(\gamma,\alpha)^3\text{H}$.

Figure 13 shows contours of the ratio between the $^7\text{Li}/\text{H}$ abundances calculated with the new and old cross sections of $^7\text{Be}(\gamma,\alpha)^3\text{He}$ and $^7\text{Li}(\gamma,\alpha)^3\text{H}$ in the parameter plane of
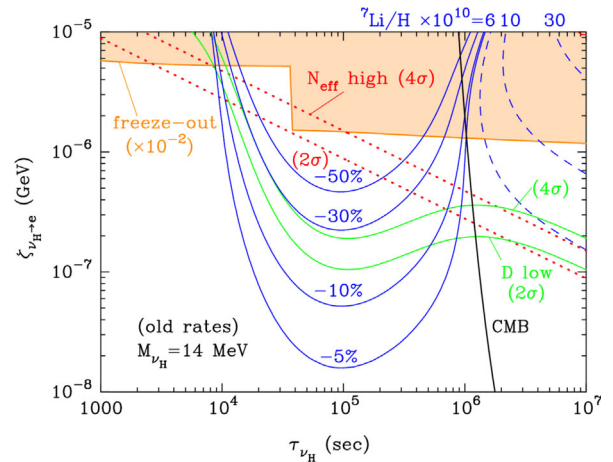

FIG. 12 (color online). Same as in Fig. 7 for $M_{\nu_H} = 14$ MeV, but the old cross sections of $^7\text{Be}(\gamma,\alpha)^3\text{He}$ and $^7\text{Li}(\gamma,\alpha)^3\text{H}$ [44] are used in the calculation.
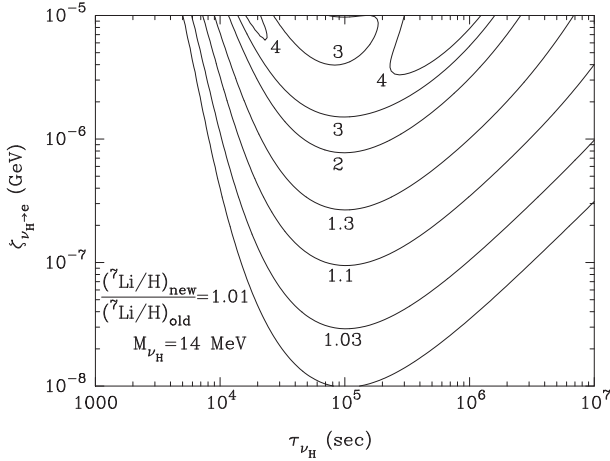
FIG. 13.   Ratio between the ^{7}Li/H abundances calculated with the new and old cross sections of ^{7}Be$(\gamma, \alpha)^3$He and ^{7}Li$(\gamma, \alpha)^3$H in the parameter plane of $(\tau_{\nu_H}, \zeta_{\nu_H \to e})$ for $M_{\nu_H} = 14$ MeV.
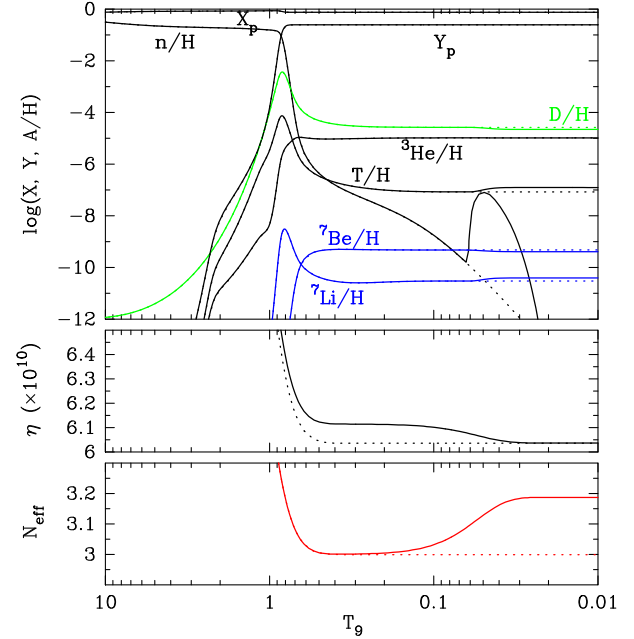

FIG. 14 (color online).   Nuclear abundances (the top panel), the baryon-to-photon ratio (the middle panel), and the effective neutrino number [Eq. (4.14)] (the bottom panel) as a function of T_9. The solid and dotted lines show results of this model with the decaying sterile neutrino and the SBBN, respectively. In the top panel, X_p and Y_p are the mass fractions of ^{1}H and ^{4}He, respectively, while abundances of other nuclides are given by ratios of number densities of nuclides and hydrogen. The mass, lifetime, and abundance of the sterile neutrino are set to be $M_{\nu_H} = 14$ MeV, $\tau_{\nu_H} = 4 \times 10^4$ s, and $\zeta_{\nu_H \to e} = 3 \times 10^{-7}$ GeV, respectively.

$(\tau_{\nu_H}, \zeta_{\nu_H \to e})$ for $M_{\nu_H} = 14$ MeV. In the parameter region at $\tau_{\nu_H} \sim 10^5$ s, the photodisintegration of ^{7}Be and ^{7}Li is efficient. Since the photodisintegration rates from the new cross sections are smaller than those from the old ones, larger abundances of ^{7}Be and ^{7}Li survive the photodisintegration. The final abundance of ^{7}Li, given by the sum of the ^{7}Be and ^{7}Li abundances, is, therefore, larger in the case of the new cross sections.

D. Parameter region for ^{7}Be destruction

We take a parameter set for the ^{7}Be destruction: $(\tau_{\nu_H}, \zeta_{\nu_H \to e}) = (4 \times 10^4 \text{ s}, 3 \times 10^{-7} \text{ GeV})$ in the case of $M_{\nu_H} = 14$ MeV.

Figure 14 shows calculated nuclear abundances (the top panel), the baryon-to-photon ratio (the middle panel), and the effective neutrino number [Eq. (4.14)] (the bottom panel) as a function of T_9. The solid and dotted lines correspond to results of the present model with the decaying sterile neutrino and the SBBN, respectively. In the top panel, X_p and Y_p are the mass fractions of ^{1}H and ^{4}He, respectively, while other curves are number densities of other nuclides relative to that of hydrogen.

In the top panel, effects of photodisintegration can be observed as differences of solid and dotted lines at $T_9 \lesssim 0.06$. The ^{7}Be nuclei are disintegrated via ^{7}Be$(\gamma, \alpha)^3$He, and the ^{7}Be abundance slightly decreases. The deuterons are also disintegrated via ^{2}H$(\gamma, n)^1$H, and the D abundance decreases and the neutron abundance increases. When the photodisintegration occurs, the temperature is already enough low that thermal nuclear reactions between charged nuclei are no longer operative. However, nonradiative neutron capture reactions are operative since no Coulomb repulsion exists in reactions with neutrons. The generated neutrons are, therefore, partially captured by ^{3}He [via ^{3}He$(n, p)^3$H] and ^{7}Be [via

^{7}Be$(n, p)^7$Li]. As a result, abundances of ^{3}H and ^{7}Li slightly increase.

In the middle panel, the baryon-to-photon ratio η decreases at $T_9 \lesssim 0.1$ because of an electromagnetic energy injection at the ν_H decay. Since the final η value is fixed to the Planck value, the baryon-to-photon ratio in the ν_H model is higher than that in SBBN at $T_9 \gtrsim 0.1$. Although this difference of the η value slightly changes BBN, differences in nuclear abundances during the BBN epoch $(T_9 \lesssim 1)$ are so small that they cannot be seen well. The downturns of the solid and dotted lines at $T_9 \gtrsim 1$ are caused by an entropy transfer from $e^\pm$ to photon at the cosmological $e^\pm$ annihilation. The η values before the $e^\pm$ annihilation are 1.68×10^{-9} in the ν_H model and 1.66×10^{-9} in the SBBN model, respectively.

In the bottom panel, the solid and dashed lines descend at $T_9 \gtrsim 1$ by the entropy transfer from $e^\pm$ to photon. The N_{eff} value is then increased at $T_9 \lesssim 0.1$ by the nonthermal neutrino injection at the ν_H decay. The final N_{eff} values after the ν_H decay are 3.19 in the ν_H model and 3 in the SBBN model, respectively.

We check the validity of the approximate formula for the final N_{eff} value. The present lifetime corresponds to

$t_{\text{eff}} = (\pi/4)\tau_{\nu_{\text{H}}} = 3.14 \times 10^4$ s (Sec. IV D 2) and $T(t_{\text{eff}}) = 6.48$ keV. The present mass corresponds to parameters of $x_{\text{m}} = 0.0365$ and $L = -13.236$ [Eq. (A18)]. The ratio of decay rates is $R_{\text{dec}} = 0.575$ [Eq. (4.8)]. The ratios of the average energies to the sterile neutrino mass in the decay mode $\nu_{\text{H}} \rightarrow \nu_e e^+ e^-$ are $f_E(\nu_e) = 0.348$, $f_E(e^-) = 0.308$, and $f_E(e^+) = 0.345$. The ratio of injected energies of neutrinos and $e^\pm$'s is then derived as $R(\nu, e) = 3.20$ [Eq. (4.9)]. The corresponding ratio of entropy densities before and after the ν_{H} decay is $S_{\gamma,\text{aft}}/S_{\gamma,\text{bef}} = 1.0129$ [Eq. (4.23)]. The effective neutrino number contributed from nonthermal neutrinos without the entropy production effect is derived as $N_{\text{eff,nt,i}} = 0.241$ [Eqs. (4.10) and (4.24)]. Taking account of the dilution associated with the entropy production, the final effective number is $N_{\text{eff}} = 3.19$ [Eq. (4.25)]. We note that a slight change in the cosmic expansion rate through a change in the g_* value by the ν_{H} was neglected in this estimation. It is thus found that this approximate estimation successfully gives the final N_{eff} value derived in our precise numerical calculation.

VII. DISCUSSIONS

A. Relic abundance of sterile neutrino

It is assumed that the sterile neutrino has a mass $M_{\nu_{\text{H}}}$ after the EW phase transition. Depending on the mixing angle, the sterile neutrinos react with standard model particles mainly via the following weak reactions:

$$\nu_{\text{H}} + \nu_e \rightarrow f + \bar{f} \tag{7.1}$$

$$\nu_{\text{H}} + f \rightarrow \nu_e + f \tag{7.2}$$

$$\nu_{\text{H}} + \bar{f} \rightarrow \nu_e + \bar{f} \tag{7.3}$$

$$\nu_{\text{H}} + e^+ \rightarrow \bar{e}_n^{\;+} + \nu_{e_n} \tag{7.4}$$

$$\nu_{\text{H}} + e^+ \rightarrow u_n^{+2/3} + \bar{d}_{n'}^{\;+1/3} \tag{7.5}$$

$$\nu_{\text{H}} + e_n^- \rightarrow e^- + \nu_{e_n} \tag{7.6}$$

$$\nu_{\text{H}} + \bar{\nu}_{e_n} \rightarrow e^- + \bar{e}_n^{\;+} \tag{7.7}$$

$$\nu_{\text{H}} + \bar{u}_n^{-2/3} \rightarrow e^- + \bar{d}_{n'}^{\;+1/3} \tag{7.8}$$

$$\nu_{\text{H}} + d_n^{-1/3} \rightarrow e^- + u_{n'}^{+2/3}, \tag{7.9}$$

where f is any fermion, i.e., charged leptons e_n [e^- ($n = 1$), μ^- ($n = 2$), and τ^- ($n = 3$)], neutrinos ν_{e_n} and up-type quarks u_n [u ($n = 1$), c ($n = 2$), and t ($n = 3$)], and down-type quarks d_n [d ($n = 1$), s ($n = 2$), and b ($n = 3$)]. In the charged current reactions, probabilities of producing respective flavors ($u_n \leftrightarrow d_{n'}$) are described by the Cabibbo-Kobayashi-Maskawa matrix [109,110].

When the weak interaction rate becomes smaller than the Hubble expansion rate, the abundance of the sterile neutrino freezes out from equilibrium. Thereafter, the ratio between the ν_{H} number density and the entropy density $Y_{\nu_{\text{H}}} \equiv n_{\nu_{\text{H}}}/s$ does not change [111]. Weak interaction rates of sterile neutrinos, ν_{H}'s, with weakly interacting standard model particles after the EW phase transition scale [56] as

$$\Gamma \sim G_{\text{F}}^2 \Theta^2 T^5, \tag{7.10}$$

where G_{F} is the Fermi constant, and $\Theta \ll 1$ is the mixing angle. The ratio between the rates and cosmic expansion rate, H, is then given [94] by

$$\begin{aligned}
\frac{\Gamma}{H} &\sim G_{\text{F}}^2 \Theta^2 T^5 \left(\frac{2\pi^{3/2}}{3\sqrt{5}} \frac{g_*^{1/2} T^2}{M_{\text{Pl}}} \right)^{-1} \\
&= \frac{3\sqrt{5}}{2\pi^{3/2}} \frac{M_{\text{Pl}} G_{\text{F}}^2 \Theta^2 T^3}{g_*^{1/2}} \\
&= 9.69 \times 10^7 \left(\frac{\Theta}{10^{-3}} \right)^2 \left(\frac{g_*}{106.75} \right)^{-1/2} \left(\frac{T}{100 \text{ GeV}} \right)^3 \\
&= 1.00 \left(\frac{\Theta}{10^{-3}} \right)^2 \left(\frac{g_*}{63.75} \right)^{-1/2} \left(\frac{T}{0.2 \text{ GeV}} \right)^3. \tag{7.11}
\end{aligned}$$

In the last line of this equation, the statistical d.o.f. of the sterile neutrino, i.e., $\Delta g_* = 2 \times 7/8$, was added to the value of $g_* = 61.75$ at $T = 200$ MeV in the standard model. A sterile neutrino with mixing angle $\Theta \sim 10^{-3}$ would thus freeze out from equilibrium at temperature $T \sim 200$ MeV. The relic abundance of ν_{H} is, therefore, given by the abundance fixed at $T \sim 200$ MeV.

The lifetime of the sterile neutrinos is roughly given [cf. Eqs. (A15) and (A27)] by

$$\begin{aligned}
\Gamma(\nu_{\text{H}} - \text{decay}) &\sim \frac{G_{\text{F}}^2 \Theta^2 M_{\nu_{\text{H}}}^5}{192\pi^3} \\
&= 1.87 \times 10^{-5} \text{ s}^{-1} \left(\frac{\Theta}{10^{-3}} \right)^2 \left(\frac{M_{\nu_{\text{H}}}}{14 \text{ MeV}} \right)^5. \tag{7.12}
\end{aligned}$$

Therefore, if a sterile neutrino with a mass $M_{\nu_{\text{H}}} \gtrsim 14$ MeV decays $\sim 10^4$–10^5 s after the big bang and reduces the primordial ^{7}Li abundance, the mixing angle would be $\Theta \sim 10^{-3}$.

The time evolution of the ν_{H} abundance has been calculated [56,93,95]. In Refs. [93,95], however, the maximal mixing angle $\Theta = \mathcal{O}(1)$ is implicitly assumed, and the dependence on the mixing angle Θ is not considered. In addition, the authors took into account only the annihilation $\nu_{\text{H}} + \bar{\nu}_{\text{H}}$ [112], which is negligibly weaker than the reactions Eqs. (7.1)–(7.9) when $\Theta \ll 1$. In Ref. [56], on the other hand, a dedicated calculation has been performed. However, the authors only focused on

shorter ν_H lifetimes of $\tau_{\nu_H} = \mathcal{O}(0.1)$ s, which correspond to relatively large values of the mixing angle $\Theta > \mathcal{O}(10^{-3})$ compared with those considered in this paper. Depending on the mixing angle, the weak reaction freeze-out of the sterile neutrino occurs in various epochs with different values of g_*. Perhaps the sterile neutrino never experiences the weak reaction equilibrium after the EW phase transition. In general, the ν_H relic abundance can sensitively depend on the evolution of sterile neutrino mass during the EW phase transition, which differs in different models of the sterile neutrino. Precise calculations of the ν_H relic abundance should be performed in detail. However, they are beyond the scope of this paper.

We estimate the freeze-out abundance of the sterile neutrino as a function of M_{ν_H} and τ_{ν_H} as follows. For a given set of $(M_{\nu_H}, \tau_{\nu_H})$, a corresponding Θ value is derived with Eq. (7.12). The temperature satisfying Eq. (7.11) is then derived with the Θ value. This temperature is defined as the freeze-out temperature T_F. An approximate value of the freeze-out abundance of ν_H is given by the equilibrium abundance at T_F. For the $T_F(M_{\nu_H}, \tau_{\nu_H})$ value, the freeze-out abundance is given by the equilibrium abundance $Y_{\nu_H,EQ}(M_{\nu_H}, T_F)$ using the following equations.

The equilibrium number density of a fermion is given [99] by

$$n_{i,EQ}(m_i, T) = \frac{g_i T^3}{2\pi^2} h(m_i/T),   (7.13)$$

where m_i and g_i are the mass and statistical d.o.f., respectively, of the fermion i, and $h(x)$ is a function given by

$$h(x) = \int_x^\infty \frac{(\epsilon^2 - x^2)^{1/2}\epsilon}{\exp(\epsilon) + 1} d\epsilon.   (7.14)$$

In the nonrelativistic limit, the function h has the limit value of $h \to 3\zeta(3)/2$. The entropy density is given [99] by

$$s(T) = \frac{2\pi^2}{45} g_{*S} T^3.   (7.15)$$

From Eqs. (7.13) and (7.14), the abundance ratio is given by

$$Y_{i,EQ}(m_i, T) \equiv \frac{n_{i,EQ}(m_i, T)}{s(T)} = \frac{45 g_i}{4\pi^4 g_{*S}} h(m_i/T).   (7.16)$$

Figure 15 shows massless d.o.f.'s in terms of energy and entropy, i.e., g_* and g_{*S}, respectively, as a function of photon temperature T. Solid lines for massless d.o.f.'s correspond to the standard model plus a sterile neutrino of mass $M_{\nu_H} = 14$ MeV and statistical d.o.f. of $g_{\nu_H} = 2$, while dashed lines correspond to the standard model. Also shown is the equilibrium abundance ratio of a sterile neutrino
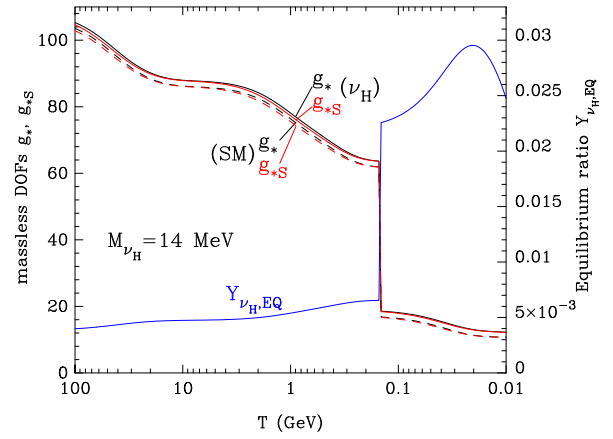

FIG. 15 (color online). Massless d.o.f.'s in terms of energy and entropy, i.e., g_* and g_{*S}, respectively, as a function of photon temperature T. Solid lines for massless d.o.f.'s correspond to the standard model plus a sterile neutrino of mass $M_{\nu_H} = 14$ MeV and statistical d.o.f. of $g_{\nu_H} = 2$, while dashed lines correspond to the standard model. Also shown is the equilibrium abundance ratio of a sterile neutrino $Y_{\nu_H,EQ}$ in the model with the sterile neutrino.

$Y_{\nu_H,EQ}$ in the model with the sterile neutrino. The massless d.o.f.'s are calculated as in Ref. [99] based on the latest data on particle mass [62]. It is assumed that the quark hadron transition occurs suddenly at temperature $T_C = 150$ MeV. Above the temperature, quarks are taken into account in the d.o.f.'s. Below the temperature, on the other hand, contributions of only hadrons are included and those of quarks are neglected. We only take into account d.o.f.'s of charged and neutral pions at $T < T_C$ since they are only relativistic hadrons.

The massless d.o.f.'s in the model with ν_H are larger than those in the model without ν_H by about 2 because of the statistical d.o.f. of the sterile neutrino. As the temperature decreases, weak bosons, heavy quarks, and leptons become nonrelativistic, and the d.o.f.'s become small. At the quark hadron transition temperature $T = T_C$, d.o.f.'s of quarks and gluons disappear, and the d.o.f.'s drastically decrease. The equilibrium abundance $Y_{\nu_H,EQ}$ increases as the temperature decreases since it is inversely proportional to the $g_{*S}(T)$ value. At T_C, the abundance significantly increases. At the lowest temperature of $T \lesssim 20$ MeV, the sterile neutrino starts to be nonrelativistic. The equilibrium abundance then decreases from this temperature.

If a light sterile neutrino with the mass $M_{\nu_H} = \mathcal{O}(10)$ MeV survives during the BBN epoch, its number density must have diluted between its weak freeze-out [$T \sim \mathcal{O}(100)$ MeV] and the BBN epoch [$T \sim \mathcal{O}(0.1)$ MeV] in order to avoid a large change of the baryon-to-photon ratio associated with the ν_H decay (see Sec. VII B). For example, we consider the case of $M_{\nu_H} = 14$ MeV and $\zeta_{\nu_H \to e} = 3 \times 10^{-7}$ GeV. This assumption corresponds to the energy ratio $\zeta_{\nu_H \to e}/\zeta_{\nu_H \to \nu} = 0.313$ [Eqs. (4.9) and (4.10)], and the

total energy injection of $\zeta_{\nu_H} = \zeta_{\nu_H \to e} + \zeta_{\nu_H \to \nu} = 1.26 \times 10^{-6}$ GeV. This energy injection is realized by the decay of sterile neutrinos with the mass $M_{\nu_H} = 14$ MeV and the number ratio $Y_{\nu_H} = 1.28 \times 10^{-5}$, where we used a relation,

$$\zeta_{\nu_H} = \frac{n_{\nu_H}}{s} \frac{s}{n_\gamma} M_{\nu_H} = 7.04 Y_{\nu_H} M_{\nu_H}, \qquad (7.17)$$

where the ratio $s/n_\gamma = 7.04$ should be measured after the cosmological $e^\pm$ annihilation. However, the freeze-out abundance is $Y_{\nu_H} = 6.56 \times 10^{-3} (g_{*S}/63.5)^{-1}$. Therefore, the sterile neutrino needs to be diluted by a factor of several hundreds.

B. Dilution of sterile neutrino

It is shown that the decays of heavier sterile neutrinos into standard model particles can realize a dilution of the light sterile neutrino ($M_{\nu_H} \sim 14$ MeV) although our naive estimate [113] suggests that a decay of a heavier sterile neutrino would result in a dilution factor smaller than required for the appropriate abundance by some factor at least. We assume that one of the heavier sterile neutrinos, i.e., ν_{H2}, predominantly contributes to the dilution or entropy production. In addition, it is assumed that the heavy neutrino dominates in terms of energy density in its decay epoch. Supposing that ν_{H2} decays into relativistic leptons and quarks which are thermalized rapidly with respect to the cosmic expansion time scale, the energy density of relativistic species after the decay is $\rho_R = \frac{\pi^2}{30} g_* T_{RH}^4$, where T_{RH} is the reheating temperature. This energy density is equal to the energy density of ν_{H2} before the decay. The ratio of the entropy per comoving volume at the epoch long after the decay (aft) to that long before the decay (bef) is given [99] by

$$\frac{S_{\text{aft}}}{S_{\text{bef}}} = \frac{g_{*S}(T_{\text{aft}}) a_{\text{aft}}^3 T_{\text{aft}}^3}{g_{*S}(T_{\text{bef}}) a_{\text{bef}}^3 T_{\text{bef}}^3}$$

$$\simeq 1.83 \langle g_*^{1/3} \rangle^{3/4} \frac{m_{\nu_{H2}} Y_{\nu_{H2}} \tau_{\nu_{H2}}^{1/2}}{M_{\text{Pl}}^{1/2}}$$

$$= 8.25 \times 10^1 \left(\frac{\langle g_*^{1/3} \rangle^{3/4}}{104^{1/4}} \right) \left(\frac{m_{\nu_{H2}}}{100 \text{ GeV}} \right)$$

$$\times \left(\frac{Y_{\nu_{H2}}}{4.00 \times 10^{-3}} \right) \left(\frac{\tau_{\nu_{H2}}}{10^{-2} \text{ s}} \right)^{1/2}, \qquad (7.18)$$

where a_j and T_j (for $j = $ bef and aft) are the scale factor and the photon temperature of the Universe at time j, and we supposed $g_* = g_{*S}$ and that the g_* and g_{*S} values do not change between the temperatures of T_{bef} and T_{aft}. We note that a large dilution factor is realized only for $M_{\nu_{H2}} \lesssim 100$ GeV. If the mass is much larger than the energy scale of the EW phase transition, the freeze-out ν_{H2}

abundance is small because of the Boltzmann suppression factor. Furthermore, the lifetime should not be longer than $\mathcal{O}(10^{-2})$ s since BBN is significantly affected by non-thermal reactions of hadronic particles generated at the ν_{H2} decay if the lifetime is longer [45]. From this equation, we find that the dilution factor, which equals the entropy enhancement factor, is about a factor of 100 at maximum. This maximum factor is ~ 3 times smaller than the necessary factor of 300. Some other mechanism of the dilution is, therefore, needed for the light sterile neutrino to destroy some moderate fraction of primordial ^{7}Be success-fully. Possible mechanisms include dilutions by massive particles other than ν_{H2} decaying into active neutrinos, $\phi \to \nu\bar{\nu}$ [114] or photons $\phi \to n\gamma$ ($n \geq 2$) [115].

In Figs. 7,9,10, and 12, parameter regions of thermal freeze-out ν_H abundances are shown by shaded regions. A possible dilution of the sterile neutrino by a factor of 100 is taken into account. The freeze-out abundances without dilutions are higher than the figure domains, and therefore not seen. The lower boundaries of these regions correspond to the abundances diluted by a factor of 100. Sudden drops of the boundaries at $\tau_{\nu_H} = 10^4$–10^5 s result from the decrease in the massless d.o.f. in terms of entropy (Fig. 15). It is clear that the parameter regions for the primordial ^{7}Li reduction are lower than the regions of freeze-out abundances. Therefore, a dilution of the sterile neutrino is necessary for the ^{7}Li reduction to work.

C. Mixing with muon and tauon neutrinos

If either a muon or tauon neutrino predominantly couples to ν_H and couplings of other charged leptons are negligible as an extreme case opposite to the case studied in this paper, effects of the sterile neutrino decay are changed. For example, we take the case of $M_{\nu_H} = 14$ MeV. The ratio of energy injections in the forms of $e^\pm$ and ν is $R(\nu, e) = 3.20$ for the coupling to ν_e, while it is $R(\nu, e) = 13.0$ for the coupling to ν_α ($\alpha = \mu$ or τ) [Eq. (4.10)]. The muon- or tauon-type mixings, therefore, result in a large energy fraction of the neutrino emitted at the decay. An $e^\pm$ injection decreases the η and N_{eff} values and induces nonthermal nucleosynthesis, while a neutrino injection increases the N_{eff} value. Therefore, a sterile neutrino that mixes only with ν_α has small effects on the primordial light element abundances and the η value relative to that on N_{eff}.

D. Constraint from pion decay

We assume that the sterile neutrino has a mass ~ 14 MeV and a lifetime $\sim 10^5$ s (parameter value for the ^{7}Li reduction), and that mixing angles of muon and tauon types, Θ_μ and Θ_τ, respectively, can be neglected. The active-sterile mixing angle is then determined to be $\Theta = \mathcal{O}(10^{-3})$ [Eqs. (7.12) and (A15)]. If the muon-type mixing is sizable, we should take into account another constraint from low energy phenomena: the sterile neutrino can be produced by the decay of charged pions, e.g., $\pi^+ \to \mu^+ + \nu_H$ or

$\pi^+ \to e^+ + \nu_H$. This channel has been searched for for a long time and many experiments gave constraints on the active-sterile mixing angle. From Ref. [116], Θ_μ^2 should be smaller than 10^{-5}. If the precision of those experiments can be improved by a few orders of magnitude, therefore, we may see a signal from pion decays, or exclude the possibility of primordial ^{7}Li reduction by ν_H suggested in this paper. Furthermore, if the muon-type mixing is of the order of $\Theta_\mu \sim 10^{-6}$, the sterile neutrino might be detected by Super Kamiokande in the future [117]. It is worth mentioning that a constraint from the supernova SN1987A observation is rather strong [56,57]; that is, roughly $\Theta^2 \lesssim \mathcal{O}(10^{-8})$ for any flavors.

VIII. SUMMARY

The primordial lithium abundance determined from spectroscopic observations of MPSs is smaller than the theoretical prediction of the SBBN model by a factor of ~ 3. It has been suggested that a BBN model with a long-lived radiatively decaying exotic particle possibly provides a solution to the Li problem. In that model nonthermal photons with energies ~ 2 MeV generated by the particle decay disintegrate ^{7}Be. The primordial ^{7}Li abundance, which is the sum of abundances of ^{7}Li and ^{7}Be produced during BBN, is then reduced. In this paper, we studied the possibility of $\mathcal{O}(10)$ MeV sterile neutrino ν_H. If it decays after BBN, and electron and positron $e^\pm$'s are emitted, the energetic $e^\pm$'s can produce energetic photons via the inverse Compton scattering of CBR. The solution to the Li problem is, therefore, also expected in this model. Then, we investigated cosmological effects of the sterile neutrino decay on primordial light element abundances, the baryon-to-photon ratio, and the effective neutrino number.

The sterile neutrino was assumed to live longer than the BBN time scale, i.e., $\gg \mathcal{O}(100)$ s. This long lifetime satisfies a recent constraint from neutrino oscillation experiments: the lifetime of a sterile neutrino lighter than the pion cannot be shorter than ~ 0.1 s. We constructed a numerical code for consistent calculations of the cosmic expansion history, BBN, and nonthermal nucleosynthesis triggered by the ν_H decaying after BBN. The updated relation between the baryon-to-photon ratio and the baryon density of the Universe is used (Sec. II A 1). The initial abundance, mass, and lifetime of the sterile neutrino were taken as free parameters. Then we formulated the injection spectrum of nonthermal photons induced by the ν_H decay (Sec. II). We introduced an active-sterile mixing angle and calculated the energy spectra of $e^\pm$'s and active neutrinos generated at the ν_H decay. Taking into account the primary photon production via the inverse Compton scattering of CBR by energetic $e^\pm$'s, and electromagnetic cascade showers induced by the primary photons, the steady state injection spectrum was derived as a function of the sterile neutrino mass and the photon temperature. Nonthermal nucleosynthesis triggered by the energetic photons is then

calculated. In this paper, we corrected errors in photodisintegration cross sections of ^{7}Be$(\gamma, \alpha)^3$He and ^{7}Li$(\gamma, \alpha)^3$H adopted in previous studies. We gave functions for the cross sections in light of recent nuclear experimental results (Sec. III). Furthermore, effects of the ν_H decay on the cosmic thermal history and evolutions of effective neutrino number and the baryon-to-photon ratio are formulated exactly (Sec. IV).

Results of our calculations are summarized as follows.

First, we calculated injection spectra of nonthermal photons as a function of the mass M_{ν_H} and photon temperature T. We took into account the energy spectra of $e^\pm$'s emitted at the decay, inverse Compton scattering of CBR by the energetic $e^\pm$'s producing primary energetic photons, and electromagnetic cascade showers induced by the primary photons. The energy spectra of $e^\pm$'s are broadly extended independent of the temperature. The energy spectra of the primary photons, on the other hand, depend significantly on the temperature, and spectra are softer at lower temperatures in the later Universe. The final injection spectra of nonthermal photons also depend on the temperature significantly. Abundances of energetic photons capable of disintegrating ^{7}Be are determined by the hardness of the primary photon spectra and the upper cutoff in the nonthermal photon spectra due to the double photon pair annihilation. We found that an effective ^{7}Be destruction can occur only if the sterile neutrino decays at $T = \mathcal{O}(1)$ keV (Sec. VI A).

Second, we simultaneously solved nonthermal nucleosynthesis induced by the nonthermal photons, and evolutions of the baryon-to-photon ratio η and the cosmological effective neutrino number N_{eff}. At the ν_H decay, energetic active neutrinos, electrons, and positrons are generated. The energies of the neutrinos are never thermalized since the weak interaction has been long since decoupled in the Universe. The nonthermal neutrinos, therefore, contribute to only the radiation energy density or the N_{eff} value. The energies of the $e^\pm$'s are, on the other hand, quickly thermalized through interactions with CBR, and eventually transferred to CBR. The comoving photon entropy is then increased. Using formulas relevant to the sterile neutrino decay (Appendix), we quantitatively solved changes of η and N_{eff} caused by the ν_H decay. The final η value is fixed to the Planck value at the cosmological recombination. Calculated results are compared with observational constraints. As a result, amounts of energy injection in the form of $e^\pm$'s at the ν_H decay are constrained from limits on primordial nuclear abundances (D and ^{7}Li), the effective neutrino number, and the CMB energy spectrum. We found a parameter region of the lifetime τ_{ν_H} and the amount of energy injection $\zeta_{\nu_H \to e}$, in which ^{7}Be is photodisintegrated and the Li problem is partially solved: $(\tau_{\nu_H}, \zeta_{\nu_H \to e}) = (10^4\text{--}10^5 \text{ s}, 10^{-6}\text{--}10^{-7} \text{ GeV})$. We also found that the sterile neutrino mass is required to be $M_{\nu_H} \gtrsim 14$ MeV. A lighter neutrino cannot destroy any significant fraction of

^{7}Be via photodisintegration without violating the constraints on the D abundance or the effective neutrino number. The best parameter region is narrow even in the case of $M_{\nu_H} \gtrsim 14$ MeV. In this parameter region, the ^{7}Be destruction by more than a factor of 3 cannot be realized since the constraint on the D abundance excludes this possibility (Sec. VI B).

Third, it was found that in the best parameter region, the ν_H decay not only decreases the η value slightly but also increases the N_{eff} value by a factor of $\Delta N_{eff} \lesssim 1$. For the moment, the 2σ ranges of the D abundance from QSO observations and the N_{eff} value from CMB observations do not indicate any effect by the sterile neutrino decay as considered in this paper. The η value at the cosmological recombination is consistent with the value at the BBN epoch inferred from measurements of primordial light element abundances, and the effective neutrino number is consistent with the case of only three active neutrinos, i.e., $N_{eff} = 3$. Since error bars on the η and N_{eff} values are getting smaller, this model for the Li reduction can be tested by future observations of the parameters η and N_{eff} (Sec. VI B).

Fourth, we compared results of the ν_H decay with the new and old cross sections of ^{7}Be$(\gamma, \alpha)^3$He and ^{7}Li$(\gamma, \alpha)^3$H. The new rates for the former and latter reactions are 2.3 and 2.5 times, respectively, larger than the corresponding old rates. The corrected cross sections thus resulted in significantly smaller efficiencies of ^{7}Be and ^{7}Li photodisintegration. Therefore, one should adopt the precise cross sections in calculations of nonthermal nucleosynthesis (Sec. VI C).

Fifth, the thermal freeze-out abundance of the sterile neutrino was estimated and compared with the best parameter region for the ^{7}Li reduction. The freeze-out abundance is much larger than the value required for the ^{7}Li reduction. Therefore, the relic sterile neutrino must be diluted before the BBN epoch by some mechanism. A sufficiently large dilution is, however, not realized by a decay of another sterile neutrino with a mass smaller than the EW scale of ~100 GeV. For example, therefore, other particles decaying before the BBN epoch are required for a successful ^{7}Be destruction associated with the ν_H decay studied in this paper (Sec. VII).

ACKNOWLEDGMENTS

APPENDIX: FORMULAS OF STERILE NEUTRINO DECAY

We derive the total decay rate of sterile neutrinos and energy spectra and average energies of electrons and positrons generated in the decay. The overall amplitude of the matrix element squared for the decay of $\nu_{HI} \to \nu_\alpha + e^- + e^+$ is given by

$$|\mathcal{M}|^2 = 32G_F^2\Theta^2[A(p_1 \cdot p_3)(p_2 \cdot p_4) + B(p_1 \cdot p_4)(p_2 \cdot p_3) + Cm_e^2(p_1 \cdot p_2)], \tag{A1}$$

where G_F is the Fermi constant; $\Theta \ll 1$ is the mixing angle; p_i is the four-momentum of particle i; the subscript i identifies the particle species as $i = 1$ for ν_{HI}, 2 for ν_α, 3 for e^-, and 4 for e^+; and constant parameters A, B, and C are defined as

$$A = (c_V + c_A)^2, \tag{A2}$$

$$B = (c_V - c_A)^2 + 4\delta_{e\alpha} + 4(c_V + c_A)\delta_{e\alpha}, \tag{A3}$$

$$C = (c_V^2 - c_A^2) + 2(c_V - c_A)\delta_{e\alpha}, \tag{A4}$$

where $c_V = -1/2 + 2\sin^2\theta_W$ and $c_A = -1/2$ are the constants for vector and axial couplings of charged leptons to the Z^0 weak boson with $\sin^2\theta_W = 0.23$ [62] the weak angle. The A term and the first terms of B and C correspond to the Z^0 exchange, while the second term of B corresponds to the $W^\pm$ exchange. The third term of B and the second term of C correspond to the interference contribution. When $\alpha = e$ is satisfied, parameter values are $A = 0.2916$, $B = 2.052$, and $C = 0.6716$.

The differential decay rate as a function of energies of e^- and e^+, i.e., E_3 and E_4, is then given by

$$\frac{d^2\Gamma}{dx_3dx_4} = \frac{G_F^2\Theta^2M_{\nu_H}^5}{64\pi^3}[Ax_3(1-x_3) + Bx_4(1-x_4) + 2Cx_m^2(2-x_3-x_4)], \tag{A5}$$

where new dimensionless variables were defined as follows: $x_m = m_e/M_{\nu_H}$ and $x_i = 2E_i/M_{\nu_H}$ [118].

The differential decay rates as a function of x_3 and x_4 are given [119] [120] by

$$\frac{d\Gamma}{dx_3} = \frac{G_F^2\Theta^2M_{\nu_H}^5}{64\pi^3}\left\{Ax_3(1-x_3)x_{f3} + B\left(\frac{x_{f3}^2}{2} - \frac{x_{f3}^3}{3}\right) + 2Cx_m^2\left[(2-x_3)x_{f3} - \frac{x_{f3}^2}{2}\right]\right\}_{x_{f3}=x_{f3,-}}^{x_{f3,+}}, \tag{A6}$$

$$\frac{d\Gamma}{dx_4} = \frac{G_F^2\Theta^2M_{\nu_H}^5}{64\pi^3}\left\{A\left(\frac{x_{f4}^2}{2} - \frac{x_{f4}^3}{3}\right) + Bx_4(1-x_4)x_{f4} + 2Cx_m^2\left[(2-x_4)x_{f4} - \frac{x_{f4}^2}{2}\right]\right\}_{x_{f4}=x_{f4,-}}^{x_{f4,+}}, \tag{A7}$$

where x_{fi} is the variable integrated in deriving Eqs. (A6) and (A7) from Eq. (A5) ($x_{f3} = x_4$ and $x_{f4} = x_3$); $x_{fi,-}$ and $x_{fi,+}$ are its minimum and maximum values, respectively;

and the terms in braces are evaluated as differences between values for $x_{\mathrm{f}i,\pm}$, i.e., $\{F(x_{\mathrm{f}i})\}_{x_{\mathrm{f}i}=x_{\mathrm{f}i,-}}^{x_{\mathrm{f}i,+}} = F(x_{\mathrm{f}i,+}) - F(x_{\mathrm{f}i,-})$. These rates are derived by integration of Eq. (A5) over $x_{\mathrm{f}i}$ in the range of $x_{\mathrm{f}i,-} \le x_{\mathrm{f}i} \le x_{\mathrm{f}i,+}$. On the other hand, the ranges of x_3 and x_4 in Eqs. (A6) and (A7), respectively, are $2x_{\mathrm{m}} \le x_i \le 1$. The values $x_{\mathrm{f}i,\pm}$ are given [119] by

$$x_{\mathrm{f}i,\pm} = \frac{(2 - x_i)(1 + 2x_{\mathrm{m}}^2 - x_i) \pm (1 - x_i)\sqrt{x_i^2 - 4x_{\mathrm{m}}^2}}{2(1 + x_{\mathrm{m}}^2 - x_i)}. \tag{A8}$$

We define dimensionless spectra as

$$\frac{d\Gamma'}{dx_i} = \left(\frac{G_{\mathrm{F}}^2\Theta^2 M_{\nu_{\mathrm{H}}}^5}{64\pi^3}\right)^{-1}\frac{d\Gamma}{dx_i}. \tag{A9}$$

Then, the following expressions are found,

$$\frac{d\Gamma'}{dx_3} = Af_1(x_3) + Bf_2(x_3) + Cf_3(x_3), \tag{A10}$$

$$\frac{d\Gamma'}{dx_4} = Af_2(x_4) + Bf_1(x_4) + Cf_3(x_4), \tag{A11}$$

where

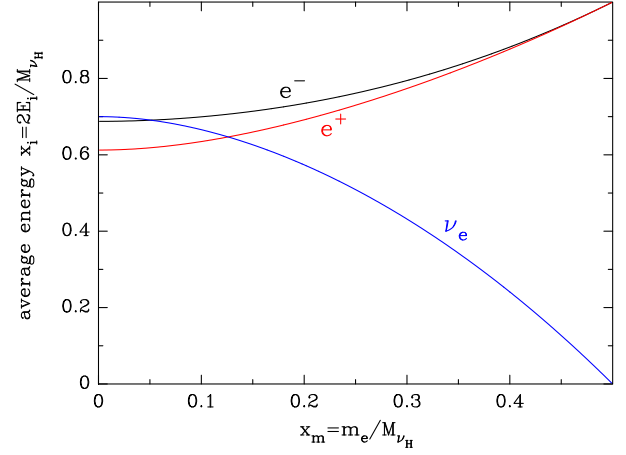$$f_1(x_i) = x_i(1 - x_i)(x_{\mathrm{f}i,+} - x_{\mathrm{f}i,-}) \tag{A12}$$

FIG. 16 (color online). Average energies of electrons, positrons, and neutrinos generated at the ν_{H} decay as a function of the mass ratio of electron and sterile neutrino.

$$f_2(x_i) = \frac{x_{\mathrm{f}i,+}^2 - x_{\mathrm{f}i,-}^2}{2} - \frac{x_{\mathrm{f}i,+}^3 - x_{\mathrm{f}i,-}^3}{3} \tag{A13}$$

$$f_3(x_i) = 2x_{\mathrm{m}}^2\left[(2 - x_i)(x_{\mathrm{f}i,+} - x_{\mathrm{f}i,-}) - \frac{x_{\mathrm{f}i,+}^2 - x_{\mathrm{f}i,-}^2}{2}\right]. \tag{A14}$$

The total decay rate is given [119,121] by

$$\Gamma(\nu_{\mathrm{H}} \to \nu_\alpha e^+ e^-) = \frac{G_{\mathrm{F}}^2\Theta^2 M_{\nu_{\mathrm{H}}}^5}{192\pi^3}\{C_1[(1 - 14x_{\mathrm{m}}^2 - 2x_{\mathrm{m}}^4 - 12x_{\mathrm{m}}^6)\sqrt{1 - 4x_{\mathrm{m}}^2} - 12x_{\mathrm{m}}^4(1 - x_{\mathrm{m}}^4)L]$$
$$+ 4C_2[x_{\mathrm{m}}^2(2 + 10x_{\mathrm{m}}^2 - 12x_{\mathrm{m}}^4)\sqrt{1 - 4x_{\mathrm{m}}^2} + 6x_{\mathrm{m}}^4(1 - 2x_{\mathrm{m}}^2 + 2x_{\mathrm{m}}^4)L]\}, \tag{A15}$$

where

$$C_1 = \frac{A + B}{4}, \tag{A16}$$

$$C_2 = \frac{C}{4}, \tag{A17}$$

$$L = \ln\left[\frac{1 - 3x_{\mathrm{m}}^2 - (1 - x_{\mathrm{m}}^2)\sqrt{1 - 4x_{\mathrm{m}}^2}}{x_{\mathrm{m}}^2(1 + \sqrt{1 - 4x_{\mathrm{m}}^2})}\right]. \tag{A18}$$

The adopted weak angle of $\sin^2\theta_{\mathrm{W}} = 0.23$ [62] corresponds to the values of $C_1 = 0.5858$ and $C_2 = 0.1679$ for the neutrino flavor of the final state $\alpha = e$.

The number spectra of the electrons and positrons emitted at the decay are given by

$$P_{e^-}(x_3) = \frac{1}{\Gamma}\frac{d\Gamma}{dx_3}, \tag{A19}$$

$$P_{e^+}(x_4) = \frac{1}{\Gamma}\frac{d\Gamma}{dx_4}. \tag{A20}$$

The total spectra of electrons and positrons are given by

$$\begin{aligned}
P_e(x) &= P_{e^-}(x) + P_{e^+}(x) \\
&= \frac{1}{\Gamma}\frac{G_{\mathrm{F}}^2\Theta^2 M_{\nu_{\mathrm{H}}}^5}{64\pi^3}\left\{(A + B)\left[\frac{x_{\mathrm{f}}^2}{2} - \frac{x_{\mathrm{f}}^3}{3} + x_{\mathrm{f}}x(1 - x)\right]\right. \\
&\quad \left.+ 2Cx_{\mathrm{m}}^2 x_{\mathrm{f}}(4 - 2x - x_{\mathrm{f}})\right\}_{x_{\mathrm{f}}=x_{\mathrm{f},-}}^{x_{\mathrm{f},+}}.
\end{aligned} \tag{A21}$$

The average energies of electrons (E_3) and positrons (E_4) are given by

$$\begin{aligned}
\bar{x}_3 &= \frac{1}{\Gamma}\int_{2x_{\mathrm{m}}}^1 x_3\frac{d\Gamma}{dx_3}dx_3 \\
&= \frac{1}{\Gamma}\frac{G_{\mathrm{F}}^2\Theta^2 M_{\nu_{\mathrm{H}}}^5}{64\pi^3}f_E(A, B, C, x_{\mathrm{m}}),
\end{aligned} \tag{A22}$$

$$\bar{x}_4 = \frac{1}{\Gamma} \int_{2x_m}^{1} x_4 \frac{d\Gamma}{dx_4} dx_4$$

$$= \frac{1}{\Gamma} \frac{G_F^2 \Theta^2 M_{\nu_H}^5}{64\pi^3} f_E(B, A, C, x_m), \tag{A23}$$

where we defined a function:

$$f_E(A, B, C, x_m) = A \left\{ \frac{1}{60} \sqrt{1 - 4x_m^2} (3 - 29x_m^2 + 48x_m^4 - 70x_m^6 - 60x_m^8) \right.$$

$$\left. - x_m^4 [(1 + x_m^2)(1 - x_m^4)L_1 + (3 - x_m^2 + x_m^4 + x_m^6)L_2] \right\}$$

$$- B \left\{ \frac{1}{60} \sqrt{1 - 4x_m^2} (9 - 52x_m^2 + 14x_m^4 + 80x_m^6 + 120x_m^8) \right.$$

$$\left. + x_m^4 [(1 - x_m^4 - 2x_m^6)L_1 + (3 + x_m^4 + 2x_m^6)L_2] \right\}$$

$$+ C \left\{ \frac{1}{6} x_m^2 \sqrt{1 - 4x_m^2} (5 - 12x_m^2 + 10x_m^4 - 12x_m^6) \right.$$

$$\left. + 2x_m^4 [(1 - x_m^2)(1 - x_m^4)L_1 + (1 + x_m^2 + x_m^4 - x_m^6)L_2] \right\}$$

$$+ (B - 2Cx_m^2) \left\{ \frac{1}{24} \sqrt{1 - 4x_m^2} (5 - 38x_m^2 + 6x_m^4 + 36x_m^6) \right.$$

$$\left. - \frac{1}{2} x_m^4 (1 + 3x_m^4)(L_1 - L_2) \right\}, \tag{A24}$$

where parameters L_1 and L_2 are defined as

$$L_1 = \ln \left[\frac{1 - 3x_m^2 - (1 - x_m^2)\sqrt{1 - 4x_m^2}}{2x_m^3} \right], \tag{A25}$$

$$L_2 = \ln \left[\frac{1 + \sqrt{1 - 4x_m^2}}{2x_m} \right], \tag{A26}$$

and $L_1 - L_2 = L$ is satisfied.

Figure 16 shows average energies of electrons, positrons, and neutrinos generated at the ν_H decay as a function of x_m calculated with Eqs. (A22) and (A23) and a trivial relation of $\bar{x}_2 = 2 - (\bar{x}_3 + \bar{x}_4)$. In the small x_m region, average energies of all three particles in the final state are close to one third of the sterile neutrino mass M_{ν_H}, i.e., $\bar{x}_i \sim 2/3$. In

the large $x_m (\lesssim 1/2)$ region, on the other hand, masses of electrons and positrons are significant fractions of the sterile neutrino mass. Most of the energy in the final state is, therefore, taken for the mass energy, and the average energy of ν_e is small.

Finally, the decay rate for the mode of $\nu_{HI} \to \sum_\beta \nu_e \bar{\nu}_\beta \nu_\beta$ is given [121] by

$$\Gamma \left(\nu_H \to \sum_\beta \nu_e \bar{\nu}_\beta \nu_\beta \right) = \frac{G_F^2 \Theta^2 M_{\nu_H}^5}{192\pi^3}. \tag{A27}$$

We note that the decay into the final state of $\nu_\alpha + \bar{\nu}_\beta + \nu_\beta$ for $\alpha = \mu$ and τ does not occur in the assumption adopted in this paper (see Sec. II C).

[1] R. A. Alpher, H. Bethe, and G. Gamow, Phys. Rev. **73**, 803 (1948).

[2] A. Coc, S. Goriely, Y. Xu, M. Saimpert, and E. Vangioni, Astrophys. J. **744**, 158 (2012).

[3] A. Coc, J.-P. Uzan, and E. Vangioni, arXiv:1307.6955.

[4] D. N. Spergel *et al.* (WMAP Collaboration), Astrophys. J. Suppl. Ser. **148**, 175 (2003).

[5] D. N. Spergel *et al.* (WMAP Collaboration), Astrophys. J. Suppl. Ser. **170**, 377 (2007).

[6] D. Larson *et al.*, Astrophys. J. Suppl. Ser. **192**, 16 (2011).

[7] G. Hinshaw, D. Larson, E. Komatsu, D. N. Spergel, C. L. Bennett, J. Dunkley, M. R. Nolta, M. Halpern *et al.*, Astrophys. J. Suppl. Ser. **208**, 19 (2013).

[8] P. A. R. Ade *et al.* (Planck Collaboration), arXiv:1303.5076 [Astron. Astrophys. (to be published)].

[9] $[A/B] = \log(n_A/n_B) - \log(n_A/n_B)_\odot$, where n_i is the number density of element ($i =$ A and B), and the subscript $\odot$ indicates the solar value.

[10] F. Spite and M. Spite, Astron. Astrophys. **115**, 357 (1982).

[11] S. G. Ryan, T. C. Beers, K. A. Olive, B. D. Fields, and J. E. Norris, Astrophys. J. **530**, L57 (2000).

[12] J. Melendez and I. Ramirez, Astrophys. J. **615**, L33 (2004).

[13] M. Asplund, D. L. Lambert, P. E. Nissen, F. Primas, and V. V. Smith, Astrophys. J. **644**, 229 (2006).

[14] P. Bonifacio *et al.*, Astron. Astrophys. **462**, 851 (2007).

[15] J. R. Shi, T. Gehren, H. W. Zhang, J. L. Zeng, and G. Zhao, Astron. Astrophys. **465**, 587 (2007).

[16] W. Aoki, P. S. Barklem, T. C. Beers, N. Christlieb, S. Inoue, A. E. G. Perez, J. E. Norris, and D. Carollo, Astrophys. J. **698**, 1803 (2009).

[17] J. I. G. Hernandez, P. Bonifacio, E. Caffau, M. Steffen, H.-G. Ludwig, N. T. Behara, L. Sbordone, R. Cayrel, and S. Zaggia, Astron. Astrophys. **505**, L13 (2009).

[18] L. Sbordone, P. Bonifacio, E. Caffau, H.-G. Ludwig, N. T. Behara, J. I. G. Hernandez, M. Steffen, R. Cayrel *et al.*, Astron. Astrophys. **522**, A26 (2010).

[19] L. Monaco, S. Villanova, P. Bonifacio, E. Caffau, D. Geisler, G. Marconi, Y. Momany, and H.-G. Ludwig, Astron. Astrophys. **539**, A157 (2012).

[20] A. Mucciarelli, M. Salaris, and P. Bonifacio, Mon. Not. R. Astron. Soc. **419**, 2195 (2012).

[21] W. Aoki, H. Ito, and A. Tajitsu, Astrophys. J. **751**, L6 (2012).

[22] W. Aoki, Memorie della Societa Astronomica Italiana Supplementi **22**, 35 (2012).

[23] L. Monaco, P. Bonifacio, L. Sbordone, S. Villanova, and E. Pancino, Astron. Astrophys. **519**, L3 (2010).

[24] Average stellar Li abundances in metal-poor globular clusters (GCs; e.g., [17,25]) are larger than those in metal-poor halo stars. The Li abundance in GC M4 turn-off stars has been determined to be $\log(^7\text{Li}/\text{H}) = -12 + (2.30 \pm 0.02 \pm 0.10)$ [25], while the Li abundance in halo dwarf stars is $\log(^7\text{Li}/\text{H}) = -12 + (2.199 \pm 0.086)$ [18]. However, these abundances are consistent with each other within the uncertainties for the moment (see Fig. 3 of Ref. [25]). The possible systematic difference in the Li abundances in GCs and the Galactic halo should be studied further in the future.

[25] A. Mucciarelli, M. Salaris, L. Lovisi, F. R. Ferraro, S. Lucatello, and R. G. Gratton, Mon. Not. R. Astron. Soc. **412**, 81 (2011).

[26] A. Frebel, W. Aoki, N. Christlieb, H. Ando, M. Asplund, P. S. Barklem, T. C. Beers, K. Eriksson *et al.*, Nature (London) **434**, 871 (2005).

[27] W. Aoki, A. Frebel, N. Christlieb, J. E. Norris, T. C. Beers, T. Minezaki, P. S. Barklem, S. Honda *et al.*, Astrophys. J. **639**, 897 (2006).

[28] B. D. Fields, Annu. Rev. Nucl. Part. Sci. **61**, 47 (2011).

[29] C. P. Deliyannis, P. Demarque, and S. D. Kawaler, Astrophys. J. Suppl. Ser. **73**, 21 (1990).

[30] M. H. Pinsonneault, T. P. Walker, G. Steigman, and V. K. Narayanan, Astrophys. J. **527**, 180 (1999).

[31] M. H. Pinsonneault, G. Steigman, T. P. Walker, and V. K. Narayanans, Astrophys. J. **574**, 398 (2002).

[32] O. Richard, G. Michaud, and J. Richer, Astrophys. J. **619**, 538 (2005).

[33] A. J. Korn, F. Grundahl, O. Richard, L. Mashonkina, P. S. Barklem, R. Collet, B. Gustafsson, and N. Piskunov, Astrophys. J. **671**, 402 (2007).

[34] K. Lind, F. Primas, C. Charbonnel, F. Grundahl, and M. Asplund, Astron. Astrophys. **503**, 545 (2009).

[35] M. Kusakabe, A. B. Balantekin, T. Kajino, and Y. Pehlivan, Phys. Rev. D **87**, 085045 (2013).

[36] D. Lindley, Mon. Not. R. Astron. Soc. **188**, 15P (1979).

[37] J. R. Ellis, D. V. Nanopoulos, and S. Sarkar, Nucl. Phys. **B259**, 175 (1985).

[38] S. Dimopoulos, R. Esmailzadeh, L. J. Hall, and G. D. Starkman, Astrophys. J. **330**, 545 (1988).

[39] J. Ellis, G. B. Gelmini, J. L. Lopez, D. V. Nanopoulos, and S. Sarkar, Nucl. Phys. **B373**, 399 (1992).

[40] M. Kawasaki and T. Moroi, Prog. Theor. Phys. **93**, 879 (1995).

[41] M. Kawasaki and T. Moroi, Astrophys. J. **452**, 506 (1995).

[42] K. Jedamzik, Phys. Rev. Lett. **84**, 3248 (2000).

[43] M. Kawasaki, K. Kohri, and T. Moroi, Phys. Rev. D **63**, 103502 (2001).

[44] R. H. Cyburt, J. R. Ellis, B. D. Fields, and K. A. Olive, Phys. Rev. D **67**, 103521 (2003).

[45] M. Kawasaki, K. Kohri, and T. Moroi, Phys. Rev. D **71**, 083502 (2005).

[46] J. R. Ellis, K. A. Olive, and E. Vangioni, Phys. Lett. B **619**, 30 (2005).

[47] K. Jedamzik, Phys. Rev. D **74**, 103509 (2006).

[48] M. Kusakabe, T. Kajino, and G. J. Mathews, Phys. Rev. D **74**, 023526 (2006).

[49] P. Minkowski, Phys. Lett. **67B**, 421 (1977).

[50] T. Yanagida, in *Proceedings of the Workshop on the Unified Theory and the Baryon Number in the Universe, Tsukuba, Japan, 1979*, edited by O. Sawada and A. Sugamoto, KEK Report No. KEK-79-18, p. 95.

[51] T. Yanagida, Prog. Theor. Phys. **64**, 1103 (1980).

[52] M. Gell-Mann, P. Ramond, and R. Slansky, in *Supergravity*, edited by D. Z. Freedom and P. van Nieuwenhuizen (North-Holland, Amsterdam, 1979).

[53] M. Fukugita and T. Yanagida, Phys. Lett. B **174**, 45 (1986).

[54] T. Asaka, S. Eijima, and H. Ishida, J. High Energy Phys. 04 (2011) 011.

[55] T. Asaka, S. Eijima, and A. Watanabe, J. High Energy Phys. 03 (2013) 125.

[56] A. D. Dolgov, S. H. Hansen, G. Raffelt, and D. V. Semikoz, Nucl. Phys. **B580**, 331 (2000).

[57] A. D. Dolgov, S. H. Hansen, G. Raffelt, and D. V. Semikoz, Nucl. Phys. **B590**, 562 (2000).

[58] L. Kawano, NASA STI/Recon Technical Report No. 92, 25163 (1992).

[59] M. S. Smith, L. H. Kawano, and R. A. Malaney, Astrophys. J. Suppl. Ser. **85**, 219 (1993).

[60] S. Sarkar, Rep. Prog. Phys. **59**, 1493 (1996).

[61] R. H. Cyburt *et al.*, Astrophys. J. Suppl. Ser. **189**, 240 (2010).

[62] J. Beringer *et al.* (Particle Data Group Collaboration), Phys. Rev. D **86**, 010001 (2012), and 2013 partial update for the 2014 edition (http://pdg.lbl.gov).

[63] A. P. Serebrov and A. K. Fomin, Phys. Rev. C **82**, 035501 (2010).

[64] G. J. Mathews, T. Kajino, and T. Shima, Phys. Rev. D **71**, 021302 (2005).

[65] A. Serebrov, V. Varlamov, A. Kharitonov, A. Fomin, Y. Pokotilovski, P. Geltenbort, J. Butterworth, and I. Krasnoschekova *et al.*, Phys. Lett. B **605**, 72 (2005).

[66] G. Steigman, J. Cosmol. Astropart. Phys. 10 (2006) 016.

[67] G. Audi, A. H. Wapstra, and C. Thibault, Nucl. Phys. **A729**, 337 (2003).

[68] D. J. Fixsen, Astrophys. J. **707**, 916 (2009).

[69] M. Kusakabe, T. Kajino, T. Yoshida, T. Shima, Y. Nagai, and T. Kii, Phys. Rev. D **79**, 123513 (2009).

[70] T. Shima, S. Naito, Y. Nagai, T. Baba, K. Tamura, T. Takahashi, T. Kii, H. Ohgaki, and H. Toyokawa, Phys. Rev. C **72**, 044004 (2005).

[71] T. Kii, T. Shima, Y. Nagai, and T. Baba, Nucl. Instrum. Methods Phys. Res., Sect. A **552**, 329 (2005).

[72] F. C. Jones, Phys. Rev. **167**, 1159 (1968).

[73] As for Eq. (51) in Ref. [41], the minus sign in the denominator of the third term on the right-hand side is different from that of Eq. (9) in Ref. [72]. We adopt the latter plus sign.

[74] E. S. Ginsberg and D. Zaborowski, Commun. ACM **18**, 200 (1975).

[75] R. J. Protheroe, T. Stanev, and V. S. Berezinsky, Phys. Rev. D **51**, 4134 (1995).

[76] V. S. Berezinskii, S. V. Bulanov, V. A. Dogiel, V. L. Ginzburg, and V. S. Ptuskin, *Astrophysics of Cosmic Rays*, edited by V. S. Verezinskii and V. L. Ginzburg (North-Holland, New York, 1990).

[77] M. Kusakabe, A. B. Balantekin, T. Kajino, and Y. Pehlivan, Phys. Lett. B **718**, 704 (2013).

[78] The electromagnetic energy injection, as considered in this paper, increases the comoving number density of background photons as a function of time. Therefore, the photon number density does not simply scale as $\propto (1 + z)^3$. Equations (2.22)–(2.28) are exact for a general case including the energy injection. Equations for dY/dz in Ref. [44] and dY/dt in Ref. [48] are, on the other hand, not exact when the effect of the electromagnetic energy injection by the exotic particle decay is significant.

[79] M. H. Reno and D. Seckel, Phys. Rev. D **37**, 3441 (1988).

[80] M. Kawasaki and M. Kusakabe, Phys. Rev. D **86**, 063003 (2012).

[81] J. M. Blatt and V. F. Weisskopf, *Theoretical Nuclear Physics* (Dover, Mineola, NY, 1991).

[82] T. Kajino, S. M. Austin, and H. Toki, Astrophys. J. **319**, 531 (1987).

[83] C. Angulo, M. Arnould, M. Rayet *et al.*, Nucl. Phys. **A656**, 3 (1999).

[84] A. di Leva, L. Gialanella, R. Kunz *et al.*, Phys. Rev. Lett. **102**, 232502 (2009).

[85] A. di Leva, L. Gialanella, R. Kunz *et al.*, Phys. Rev. Lett. **103**, 159903 (2009).

[86] M. Carmona-Gallardo, B. S. Nara Singh, M. J. G. Borge *et al.*, Phys. Rev. C **86**, 032801 (2012).

[87] C. Bordeanu, G. Gyürky, Z. Halász, T. Szücs, G. G. Kiss, Z. Elekes, J. Farkas, Z. Fülöp, and E. Somorjai, Nucl. Phys. **A908**, 1 (2013).

[88] P. D. Parker and R. W. Kavanagh, Phys. Rev. **131**, 2578 (1963).

[89] T. A. Tombrello and P. D. Parker, Phys. Rev. **131**, 2582 (1963).

[90] Q. K. K. Liu, H. Kanada, and Y. C. Tang, Phys. Rev. C **23**, 645 (1981).

[91] C. E. Waltham, S. H. Chew, J. Lowe, J. M. Nelson, and A. R. Barnett, Nucl. Phys. **A395**, 119 (1983).

[92] R. H. Cyburt and B. Davids, Phys. Rev. C **78**, 064614 (2008).

[93] R. J. Scherrer and M. S. Turner, Astrophys. J. **331**, 19 (1988); **331**, 33 (1988).

[94] G. M. Fuller, C. T. Kishimoto, and A. Kusenko, arXiv:1110.6479.

[95] E. W. Kolb and R. J. Scherrer, Phys. Rev. D **25**, 1481 (1982).

[96] V. F. Shvartsman, Sov. Phys. JETP Lett. **9**, 184 (1969).

[97] G. Steigman, D. N. Schramm, and J. E. Gunn, Phys. Lett. **66B**, 202 (1977).

[98] J. L. Feng, A. Rajaraman, and F. Takayama, Phys. Rev. D **68**, 063504 (2003).

[99] E. W. Kolb and M. S. Turner, *The Early Universe* (Addison-Wesley, Reading, MA, 1990).

[100] We should take into account only the photon as a relativistic species in thermal and chemical contact with $e^{\pm}$'s and photons themselves during the cosmic epoch after BBN. This is because light active neutrinos had been decoupled from the thermal bath before the onset of BBN at $T \sim 1$ MeV. We note that previous studies (e.g., [35,98]) are erroneous since the g_{*S} factor included the contribution from neutrinos. The right numerical value in the following Eq. (4.23) is then higher than the previous suggestion by a factor of $3.91/2 = 1.96$.

[101] W. Hu and J. Silk, Phys. Rev. Lett. **70**, 2661 (1993).

[102] We derived this effective time [48], which is different from $t_{\rm eff} = [\Gamma(\beta)]^{1/\beta}\tau_{\nu_{\rm H}}$ in Ref. [101].

[103] M. Pettini and R. Cooke, Mon. Not. R. Astron. Soc. **425**, 2477 (2012).

[104] T. M. Bania, R. T. Rood, and D. S. Balser, Nature (London) **415**, 54 (2002).

[105] Y. I. Izotov and T. X. Thuan, Astrophys. J. **710**, L67 (2010).

[106] E. Aver, K. A. Olive, and E. D. Skillman, J. Cosmol. Astropart. Phys. 05 (2010) 003.

[107] K. Lind, J. Melendez, M. Asplund, R. Collet, and Z. Magic, Astron. Astrophys. **554**, A96 (2013).

[108] D. J. Fixsen, E. S. Cheng, J. M. Gales, J. C. Mather, R. A. Shafer, and E. L. Wright, Astrophys. J. **473**, 576 (1996).

[109] N. Cabibbo, Phys. Rev. Lett. **10**, 531 (1963).

[110] M. Kobayashi and T. Maskawa, Prog. Theor. Phys. **49**, 652 (1973).

[111] We note that this ratio $Y_{\nu_{\rm H}}$ is measured in a unit different from that of nuclear mole fractions Y_A introduced in Sec. II G.

[112] D. A. Dicus, E. W. Kolb, and V. L. Teplitz, Astrophys. J. **221**, 327 (1978).

[113] T. Asaka, M. Laine, and M. Shaposhnikov, J. High Energy Phys. 01 (2007) 091.

[114] S. Hannestad, Phys. Rev. D **70**, 043506 (2004).

[115] K. Ichikawa, M. Kawasaki, and F. Takahashi, Phys. Rev. D **72**, 043522 (2005).

[116] A. Kusenko, S. Pascoli, and D. Semikoz, J. High Energy Phys. 11 (2005) 028.

[117] T. Asaka and A. Watanabe, J. High Energy Phys. 07 (2012) 112.

[118] We note that coefficients of Eq. (A9) in Ref. [119] are erroneous.

[119] L. M. Johnson, D. W. McKay, and T. Bolton, Phys. Rev. D **56**, 2970 (1997).

[120] Equation (A10) of Ref. [119] should be multiplied by 1/4 after coefficients are corrected.

[121] D. Gorbunov and M. Shaposhnikov, J. High Energy Phys. 10 (2007) 15.